Ore Geology Reviews 92 (2018) 416–429

Contents lists available at ScienceDirect

Ore Geology Reviews

journal homepage: www.elsevier.com/locate/oregeorev

He, Ar, and S isotopic constraints on the relationship between A-type granites and tin mineralization: A case study of tin deposits in the Tengchong–Lianghe tin belt, southwest China

Xiao-Cui Chen[a,*], Cheng-Hai Zhao[b], Jing-Jing Zhu[b], Xin-Song Wang[b], Tao Cui[a]

[a] Guizhou Institute of Technology, Guiyang 550003, China
[b] State Key Laboratory of Ore Deposit Geochemistry, Institute of Geochemistry, Chinese Academy of Sciences, Guiyang 550005, China

ARTICLE INFO

Keywords:
Tengchong–Lianghe tin belt
He, Ar, and S isotopes
Ore-forming fluids
A-type granite

ABSTRACT

The Tengchong–Lianghe tin belt in western Yunnan Province, southwest China, is the most important tin mineralization belt in the Sanjiang Tethyan Metallogenic Domain (STMD). There are two large tin deposits in this belt: the Paleogene Lailishan and the Late Cretaceous Xiaolonghe deposits. The two deposits are spatially and temporally associated with the Lailishan and Xiaolonghe granitic plutons, respectively. Recent studies suggest that the Lailishan and Xiaolonghe granitic plutons exhibit most of the mineralogical and geochemical characteristics of A-type granites. In this study, we discuss the He, Ar, and S isotopes of pyrite samples from the two large tin deposits to trace ore-forming fluids and elements. We also review the relationship between A-type granites and tin deposits from a new perspective. The $\delta^{34}S_{CDT}$ values of the Lailishan tin deposit range from +4.9‰ to +6.7‰, with an average value of +5.53‰. The $\delta^{34}S_{CDT}$ values of the Xiaolonghe tin deposit range from +5.0‰ to +8.1‰, with an average value of +6.33‰. These values are slightly higher than those of the granites (0‰ to +5.7‰) in the Tengchong–Lianghe area, indicating mainly magmatic sources for the sulfur of ore-forming fluids with a small amount of S from the wall rocks. The Lailishan tin deposit has $^{3}He/^{4}He$ values of 1.57–3.46 Ra, with an average value of 2.078 Ra, and $^{40}Ar/^{36}Ar$ values of 382.00–622.99, with an average value of 459.67. The Xiaolonghe tin deposit has $^{3}He/^{4}He$ values of 0.53–0.88 Ra, with an average value of 0.686 Ra, and $^{40}Ar/^{36}Ar$ values of 301.06–348.43, with an average value of 322.04. These values suggest that ore-forming fluids of the Lailishan and Xiaolonghe tin deposits have mixed crustal, mantle, and a small volume of meteoric water sources in different proportions. The mantle ^{4}He values and $^{3}He/^{4}He$ values of the Lailihsan tin deposit (26–44%, 1.57–3.46 Ra) are markedly higher than those of the Xiaolonghe tin deposit (8–15%, 0.53–0.88 Ra), implying increased crust–mantle interaction in the Paleogene relative to the Late Cretaceous in western Yunnan. This interaction may be attributed to the upwelling of the asthenosphere through the break-off of the Neo-Tethyan slab during the main collisional period (65–41 Ma) of India–Asia.

1. Introduction

Janecka and Stemprok (1967) argued that 82% of the global tin deposits are associated with granites. The spatial and temporal relationship between tin mineralization and granitic rocks is well documented in many studies pertaining to mineral deposits that have been conducted worldwide (Zaw, 1990; Taylor and Wall, 1992, 1993; Schwartz et al., 1995; Mao et al., 2004; Peng et al., 2007). Tin (Sn) mineralization is traditionally considered to be associated with S-type granites because their magmatic differentiation can produce voluminous Sn-enriched ore-forming fluids (Heinrich, 1990; Stemprok, 1990; Taylor and Wall, 1993). Recently, a number of tin deposits were considered to be genetically related to A-type granites in some regions such as Nigeria, Brazil, America, and China (in Sinkiang together with Nanling). This finding redirected the focus on tin deposits and tin mineralization to more types of granites (Taylor, 1976; Bi et al., 1992; Botelho and Moura, 1998; Payolla et al., 2002; Haapala and Lukkari, 2005; Jiang et al., 2006; Li et al., 2007; Moura et al., 2007; Bi et al., 2008; Konopelko et al., 2009; Neto et al., 2009; Gonevchuk et al., 2010; Yang et al., 2010; Lamarao et al., 2012; Zhao et al., 2013). However, the relationship between tin mineralization and A-type granites is not yet well understood, and only a few systematic studies have investigated this relationship.

The Sanjiang Tethyan Domain in southwestern China is tectonically

* Corresponding author at: School of Resource and Environmental Engineering, Guizhou Institute of Technology, 1 Caiguan Road, Guiyang 550003, China.
E-mail address: cxchyh@163.com (X.-C. Chen).

https://doi.org/10.1016/j.oregeorev.2017.11.032
Received 15 March 2017; Received in revised form 28 November 2017; Accepted 29 November 2017
Available online 02 December 2017

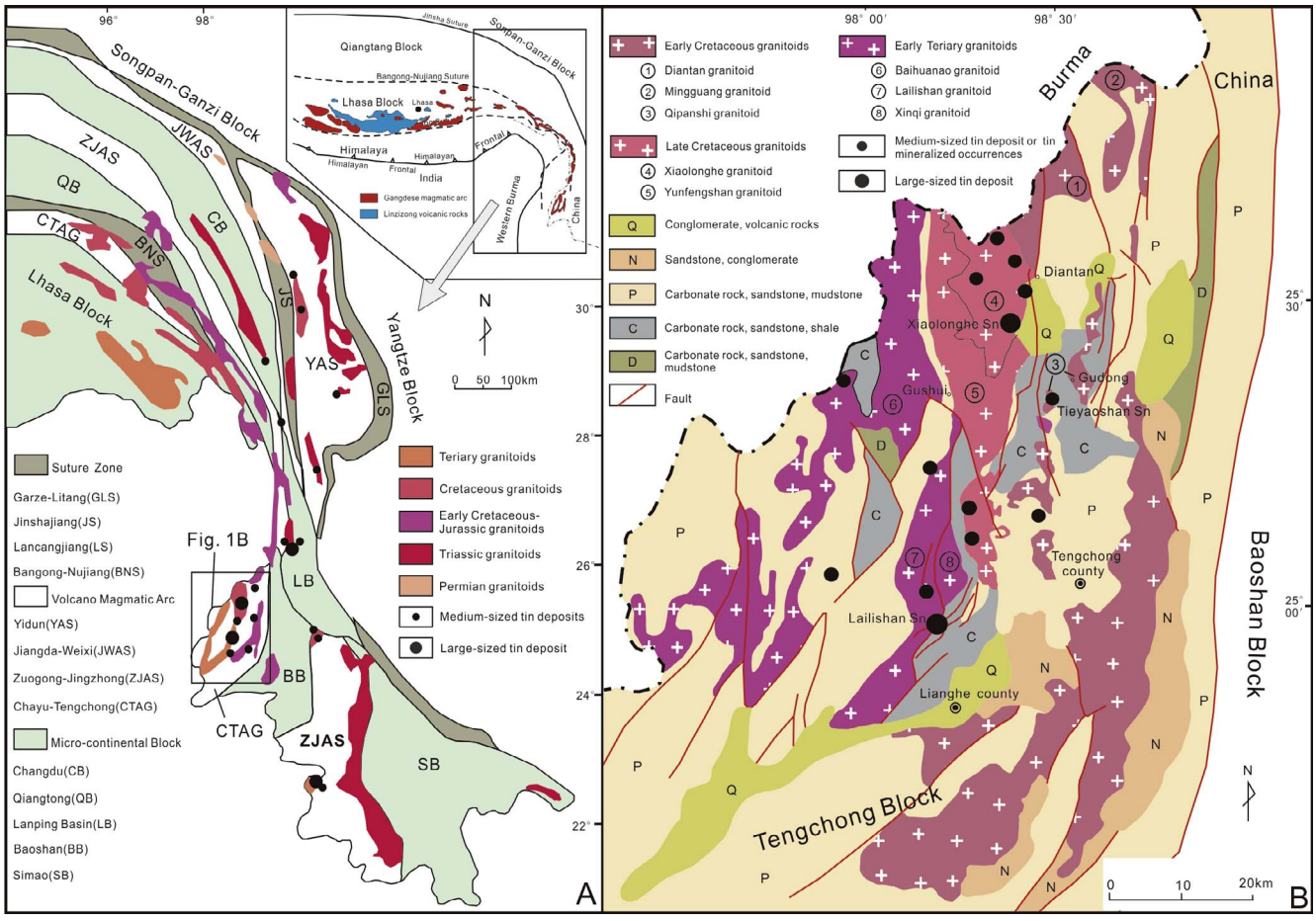

Fig. 1. (A) Tectonic framework and distribution of magmatic rocks as well as tin deposits in the Sanjiang Tethyan Domain (modified by Hou et al. (2007), Chung et al. (2005), and Xu et al. (2012)); (B) Schematic showing the distribution of magmatic rocks and tin deposits in the Tengchong–Lianghe tin belt (modified after Chen (1987), Hou et al. (2007)). Abbreviations: Q: Quaternary; N: Neogene; P: Permian; C: Carboniferous; D: Devonian.

a part of the southeast segment of the East Tethyan tectonic domain. It is in the eastern part of the Tethyan–Himalayan tectonic belt within southeast Asia (Fig. 1A) (Searle et al., 1987; Yin and Harrison, 2000; Hou et al., 2007; Wu et al., 2008). The Tengchong–Lianghe tin belt, in western Yunnan, southwest China, is the most important polymetallic tin belt in the Sanjiang Tethyan Metallogenic Domain (STMD). In addition, this tin belt, which is adjacent to Burma, has been suggested to be the northernmost continuation of the South-East Asian giant tin belt (Taylor, 1979; Clarke and Beddoe-Stephens, 1987). There are two large tin deposits (Lailishan and Xiaolonghe, with more than 50,000 tonnes of Sn), five medium-sized tin deposits (with 30,000–50,000 tonnes of Sn), and numerous mineralized localities in this tin belt. Tin mineralization is spatially associated with granitoids. Three N-S trending granitic belts were recognized in the Tengchong–Lianghe region, with emplacement ages of Early Cretaceous, Late Cretaceous, and Early Cenozoic (Chen, 1987; Yang et al., 2009; Li et al., 2012; Xu et al., 2012; Chen et al., 2015). The large Lailishan and Xiaolonghe tin deposits are spatially associated with the Lailishan and Xiaolonghe granitic plutons, respectively (Chen et al., 2014, 2015) (Fig. 1B). Recent systematic studies of the Lailishan and Xiaolonghe granitic plutons have suggested that the two granitic plutons have characteristics of A-type granites (Jiang et al., 2012; Zhang et al., 2013; Chen et al., 2015; Lin et al., 2015). In fact, tin-related A-type granites were also discovered in other regions of the SE Asian giant tin belt such as Burma and Malaysia (Ng et al., 2015; Jiang et al., 2016), as well as the eastern Lhasa terrane (Qu et al., 2002, 2012; Lin et al., 2012). We have previously reported the temporal link between tin mineralization and the emplacement of A-type granites in the Tengchong–Lianghe tin belt (Chen et al., 2014, 2015). However, few reliable and systematic geochemical studies characterizing the ore-forming fluids and material sources of the tin deposits of this belt exist.

Helium and argon isotopes show a unique advantage in identifying fluid sources owing to their steady behavior and distinct isotopic concentrations in various geochemical reservoirs (e.g., crust and mantle) (Ozima and Podosek, 2001; Ballentine and Burnard, 2002). The $^{3}He/^{4}He$ values of mantle-derived fluids are 1000 times greater than those of crust-derived fluids. The $^{3}He/^{4}He$ ratios of crust-derived fluids range from 0.01 Ra to 0.05 Ra (Stuart et al., 1995), whereas those of mantle-derived fluids vary from 6 Ra to 7 Ra (Dunai and Baur, 1995). This vast difference in He isotopic ratios makes it even easier to identify minor mantle-derived He in fluids (Stuart et al., 1995; Hu et al., 1998, 2009, 2012; Sun et al., 2009). Thus, helium and argon isotopes can be used to distinguish the sources of hydrothermal fluids in ore deposits (Hu et al., 1999, 2004, 2009, 2012; Li et al., 2007; Sun et al., 2009; Wu et al., 2011; Burnard, 2012; Zhu et al., 2013a; Xu et al., 2014; Zhai et al., 2015). Furthermore, the research of helium and argon coupled with sulfur isotopes is of great significance in tracing ore-forming fluids and understanding the genesis of ore deposits.

In this study, we discuss noble gases (He and Ar) as well as sulfur isotopic data for the Lailishan and Xiaolonghe tin deposits in the Tengchong–Lianghe tin belt with the aim of deciphering the origin of the hydrothermal fluids and their connection with deep sources, e.g., the mantle. These isotopic data may shed light on tin mineralization and its relationship to A-type granites.

2. Geological setting

2.1. Tectonic and geological background

The STMD is tectonically a part of the southeastern segment of the Tibetan Plateau (Fig. 1A). The geological evolution of the Tibetan Plateau involves plate convergence, collision, and accretion from the Paleozoic to the Cenozoic period. It is related to the opening and closing of successive Tethyan ocean basins as well as the subsequent ongoing collision between the Indian and Asian continents (Şengör, 1984, 1987; Metcalfe, 1996, 2013; Wang et al., 2013). The Tibetan Plateau comprises a number of diverse exotic blocks separated by different sutures formed at different times (Fig. 1A). The Indian Plate and the Lhasa block are separated by the Yarlung–Tsangpo suture zona, whereas the Lhasa block is separated from the Qiangtang terrane by the Bangong–Nujiang suture zone. During the Late Triassic–Late Jurassic period, the northward shift of the Lhasa and west Burma blocks resulted in the subduction of the Meso-Tethys as well as the formation of Neo-Tethys (Metcalfe, 1996, 2002; Bortolotti and Principi, 2005). The closure of Meso-Tethys, which formed the Bangong–Nujiang suture, occurred during the Late Jurassic and Early Cretaceous (Searle et al., 1987; Yin and Harrison, 2000; Kapp et al., 2005). The closure of the Neo-Tethys formed the Yarlung–Tsangpo suture and occurred after the Late Cretaceous; then, the India–Eurasia collision created the Tibetan Plateau. The age of the collision between India and Asia remains moot and estimates range from the Late Cretaceous (> 65 Ma) to as recently as the Oligocene (34 Ma) (Searle et al., 1997; Yin and Harrison, 2000; Leech et al., 2005; Zhu et al., 2005; Najman, 2006; Aitchison et al., 2007; Mo et al., 2007, 2008). The Tethyan ocean subduction and the collision between the Indian and Asian continents induced widespread magmatism and mineralization, thus creating the Tethyan metallogenic belt, one of three giant metallogenic belts in the world (i.e., the Tethyan, Palaeo-Asian, Circum-Pacific) (Hou et al., 2007).

The STMD is an important part of the Tethyan metallogenic belt as it is characterized by its unique tectonic setting, variety of mineralization styles and complex deposit types. Tin mineralization in the STMD mainly occurred in western Yunnan, eastern Tibet, and western Sichuan (Fig. 1A) (Shi et al., 1991; Hou et al., 2007; Chen et al., 2014). The Tengchong–Lianghe tin belt is located in western Yunnan (Fig. 1A, B) and is the most important polymetallic tin district in the STMD. The tin belt, which is east of the China–Burma border (Fig. 1A), is also the northernmost continuation of the SE Asian giant tin belt (Taylor, 1979; Clarke and Beddoe-Stephens, 1987). Approximately 54% of the world's tin production is from the SE Asian tin belt, which is a N-S oriented, 2800-km-long and 400-km-wide tin belt. It extends from southwest China, Burma (Myanmar), and Thailand to Peninsular Malaysia as well as the Indonesian tin islands (Taylor, 1979; Schwartz et al., 1995). The Tengchong–Lianghe tin belt is in the Tengchong–Baoshan block, which is generally considered the northeast part of the Sibumasu block (Şengör, 1979, 1984; Metcalfe, 1984, 1988; Cong et al., 1993; Metcalfe, 2000, 2002). The Sibumasu block is a contiguous continental block that extends from the Tengchong–Baoshan block in western Yunnan and eastern Burma through western Thailand, western Peninsular Malaysia, and northeastern Sumatra (Ueno, 2003; Burchfiel and Chen, 2012; Metcalfe, 2013). Jiang et al. (2017) recognized two Late Cretaceous tin–tungsten-related A-type granites on the southern segment of the Sibumasu block within Burma. Actually, A-type granites and associated tin mineral systems were also recently recognized in the STMD, such as the Tengchong–Lianghe tin belt (Jiang et al., 2012; Zhang et al., 2013; Chen et al., 2015; Lin et al., 2015) and the eastern Lhasa terrane (Qu et al., 2002, 2012; Lin et al., 2012). These provided new insights into the types of granites and related tin mineralization in this region.

The Tengchong–Lianghe tin belt consists of two large tin deposits (Lailishan and Xiaolonghe, with more than 50,000 tonnes of Sn), five medium-sized tin deposits (30,000 tonnes to 50,000 tonnes of Sn), and nearly one hundred mineralized localities. The tin deposits are all spatially associated with granites (Fig. 1B). At least three N-S-trending granitoid belts have been recognized in this area (Fig. 1B): Paleogene granitoids, Late Cretaceous granitoids, and Early Cretaceous granitoids (Chen et al., 1987; Hou et al., 2007; Xu et al., 2012; Chen et al., 2015). The Paleogene granitoids are the Xinqi, Lailishan, and Baihuanao, with emplacement ages ranging from 51.1 Ma to 59.8 Ma based on U–Pb data (Xu et al., 2012; Chen et al., 2015). The large Lailishan tin deposit is spatially related to the Lailishan granite (Fig. 1B). The Late Cretaceous granitoids include two major granite plutons (Xiaolonghe and Yunfengshan) with U–Pb ages between 68 Ma and 76 Ma (Xu et al., 2012; Chen et al., 2015). The large Xiaolonghe tin deposit is associated with the Xiaolonghe granite (Fig. 1B). The Early Cretaceous granitoids are divided into three major plutons (Diantan, Mingguang, and Qipanshi), with emplacement ages between 100 Ma and 143 Ma based on U–Pb data (Cong et al., 2010; Li et al., 2012; Xu et al., 2012). Our previous studies have suggested that the Lailishan and Xiaolonghe tin deposits formed during the Paleogene (48–53 Ma) and Late Cretaceous (71–74 Ma), respectively (Chen et al., 2014). The ore-forming ages of the two deposits are highly consistent with the zircon U–Pb ages of the host Lailishan (ca. 53 Ma) and Xiaolonghe (ca. 73 Ma) granites (Chen et al., 2015). The Paleogene granites in which the Lailishan tin deposit occurs and the Late Cretaceous granites in which the Xiaolonghe tin deposit occurs exhibit most of the mineralogical and geochemical characteristics of A-type granites (Jiang et al., 2012; Zhang et al., 2013; Chen et al., 2015; Lin et al., 2015).

2.2. Deposit geology

The Lailishan tin deposit has Sn reserves of approximately 58,000 tonnes, with an average Sn grade of 0.66% (Liu et al., 2005). The major sedimentary strata exposed in the Lailishan tin ore district are carbonaceous metasedimentary rocks. The most prominent structures are NE- and NS-trending faults. These structures control the distribution of granitic intrusions as well as the associated tin mineralization. Ore bodies mainly occur in the outer contact zones of the Lailishan granite or the fractured zones surrounding the granitic intrusion (Fig. 2A). In this deposit, the ore bodies strike 40°–80° along the NE-trending structures. The main ore bodies belong to the V-57, V-36, and V-10 groups; however, only the latter is presently being exploited. The main ore bodies of the V-10 group are 130–440 m long and 100–250 m deep. Two types of mineralization are identified in the Lailishan tin ore district: the upper oxidized ore zone and the lower primary mineralization zone. The upper oxidized ore zone, part of which composed of the V-36 and V-57 groups, has been mainly strip-mined (Fig. 3A). The ore types of the upper oxidized ore belt are mainly skarn and quartz–sulfide associated with the massive mineralization at the outer contact zone between the granites and surrounding rocks. The lower primary mineralization zone, part of which is composed of the V-36 and V-10 groups, forms the majority of the ore bodies in the Lailishan tin ore district. Tin mineralization mainly occurs in the inner or outer contact zones between the granites and surrounding rocks or the fracture zone in the wall rocks (Fig. 3B). We identified three ore types in the lower primary mineralization zone based on mineral association and occurrence: greisen, quartz–sulfide, and skarn. The greisen-type ores mainly comprise cassiterite, quartz, topaz, muscovite, and fluorite (Fig. 3a1, a2). It is the richest reserve with a grade of approximately 60 wt%, and it accounts for 30%–50% of the total tin reserves. Cassiterite and muscovite in the ore have a radial shape (Fig. 3a2). The quartz–sulfide ore comprises cassiterite, quartz, pyrite, and minor sericite (Fig. 3b1, b2). Cassiterite is coarse-grained with grains up to hundreds of micrometers in length; some cassiterite grains typically have a short prismatic and bipyramidal shape (Fig. 3b2). The skarn ore mainly consists of garnet, pyrite, and cassiterite; however, it is rare compared to the other two ores. Garnet grains grow up to a few centimeters in length and pyrite grains have a colloidal structure (Fig. 3c1, c2). Cassiterite in all ore types is light to dark brown, mostly euhedral to subhedral, and tens

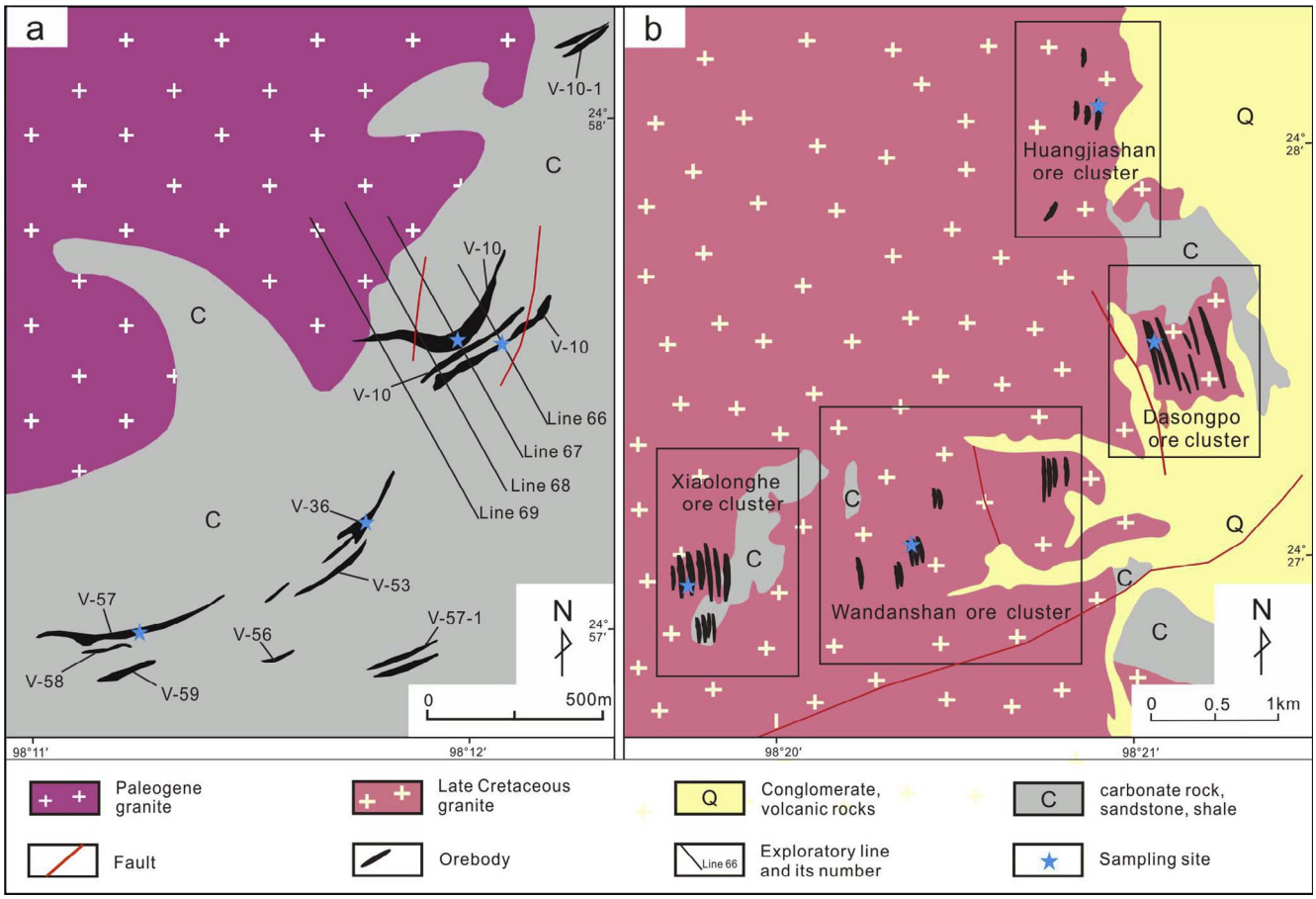

Fig. 2. Simplified geological map of the (A) Lailishan and (B) Xiaolonghe tin deposits. The main ore bodies of the Lailishan tin deposit belong to the V-57, V-36, and V-10 groups. The Xiaolonghe tin deposit comprises four ore clusters: Xiaolonghe, Wandanshan, Dasongpo, and Huangjiashan.

to hundreds of micrometers in length (Fig. 3). CL images clearly show oscillatory zoning, whereas BSE images show that cassiterite has a higher luminance compared to that of the other minerals (Fig. 4a1, a2). The hydrothermal alteration of the Lailishan tin deposit includes, but is not limited, to greisenization, pyritization, skarnitization, silicification, chloritization, and carbonatization. Tin mineralization is mainly associated with greisen, pyritic, and skarn alteration.

The Xiaolonghe tin deposit is the largest in the Tengchong–Lianghe tin belt with Sn reserves of more than 65,600 tonnes (Liu et al., 2005). Many granitoids are present in the Xiaolonghe tin ore district, with minor carbonaceous metasedimentary rocks at the top of some (Fig. 2B). The most prominent structures in the Xiaolonghe tin ore district are the N-S- and NW-W-trending faults. Ore bodies mainly occur at the top and sides of the granite or the contact zones between the Xiaolonghe granite unit and the surrounding rocks (Fig. 5A). In this deposit, the ore bodies trend nearly N-S, controlled by the N-S-trending structures (Fig. 5B). The ore bodies significantly vary in size, ranging in length from 30 m to 300 m and in thickness from 1 m to 20 m. There are four ore clusters (Xiaolonghe, Wandanshan, Dasongpo, and Huangjiashan; Fig. 2B) in the Xiaolonghe tin ore district. Each ore cluster has typical ore types based on mineral association and occurrence. The ore bodies of the Xiaolonghe ore cluster are mainly in the interior of the Xiaolonghe granitic pluton (Fig. 5a1). Tin mineralization is dominated by greisen vein-type ores, with coexisting quartz, muscovite, and cassiterite (Fig. 5a1, a2). CL images show that the cassiterite grains have clearly visible oscillatory zoning, and the BSE images show that cassiterite has a brighter luminance compared to other minerals (Fig. 4b1, b2). The quartz–sulfide-type ores mainly occur in the outer contact zones between the granite and surrounding rocks in the Wandanshan ore cluster, which mainly comprises cassiterite, quartz, and pyrite (Fig. 5b1, b2). Cassiterite grains are dark brown with clearly visible oscillatory zoning (Fig. 5b2). The ore bodies in the Dasongpo ore cluster are mainly in the inner contact zone between the granite and surrounding rocks. The main tin mineralization is dominated by greisen-type ores of cassiterite, muscovite, quartz, and pyrite (Fig. 5c1, c2). The ore bodies of the Huangjiashan ore cluster are in the interior or edges of the granitic pluton (Fig. 5d1). The main tin mineralization is dominated by greisen vein-type ores, with quartz, muscovite, and cassiterite in veins within the granitoids (Fig. 5d1, d2). As noted for the Lailishan deposit, the hydrothermal alteration of the Xiaolonghe tin deposit comprises processes that include but are not limited to greisenization, pyritization, and carbonatization. Tin mineralization is mainly associated with greisen, pyritic alteration, and silicification.

3. Analytical methods

3.1. Sample collection and preparation

A total of forty-two pyrite samples were collected for sulfur isotopic analysis from the two tin deposits. Ten of these samples were collected from the V-10, V-36, and V-57 ore groups of the Lailishan tin deposit. Of the ten samples, six were prepared for He and Ar isotopic analysis. The remaining thirty-two samples were collected from the four ore clusters of the Xiaolonghe tin deposit with the following specifics: 1) ten samples from the Xiaolonghe ore cluster, three of which were prepared for He and Ar isotopic analysis; 2) six samples from the Wandanshan ore cluster, two of which were prepared for He and Ar isotopic analysis; 3) nine samples from the Dasongpo ore cluster, three of which were prepared for He and Ar isotopic analysis; and 4) seven samples from the Huangjiashan ore cluster, two of which were prepared

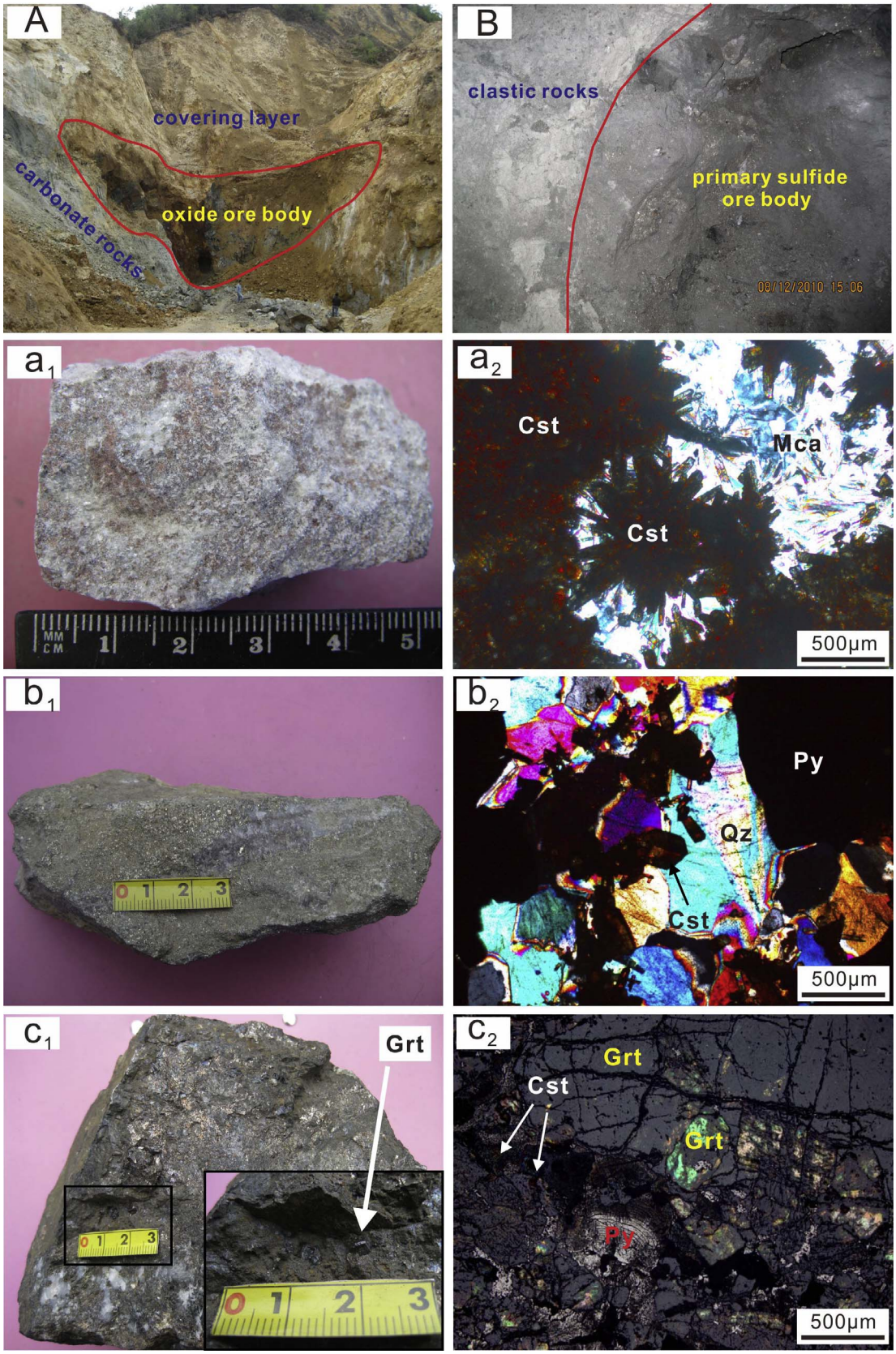

Fig. 3. Images of the ore bodies and mineral assemblages in the Lailishan tin deposit. (A) Field photo of the strip mining of the upper oxidized ore belt; (B) Images of the primary sulfide ore body in the lower mineralization belt; (a_1 and a_2) greisen-type ore with cassiterite and muscovite in radial shape; (b_1 and b_2) quartz–sulfide-type ore with prismatic and bipyramidal cassiterite crystals; (c_1 and c_2) skarn-type ore with garnet grains of several centimeters. Abbreviations: Cst: cassiterite; Py: pyrite; Mca: muscovite; Qz: quartz; Grt: garnet.

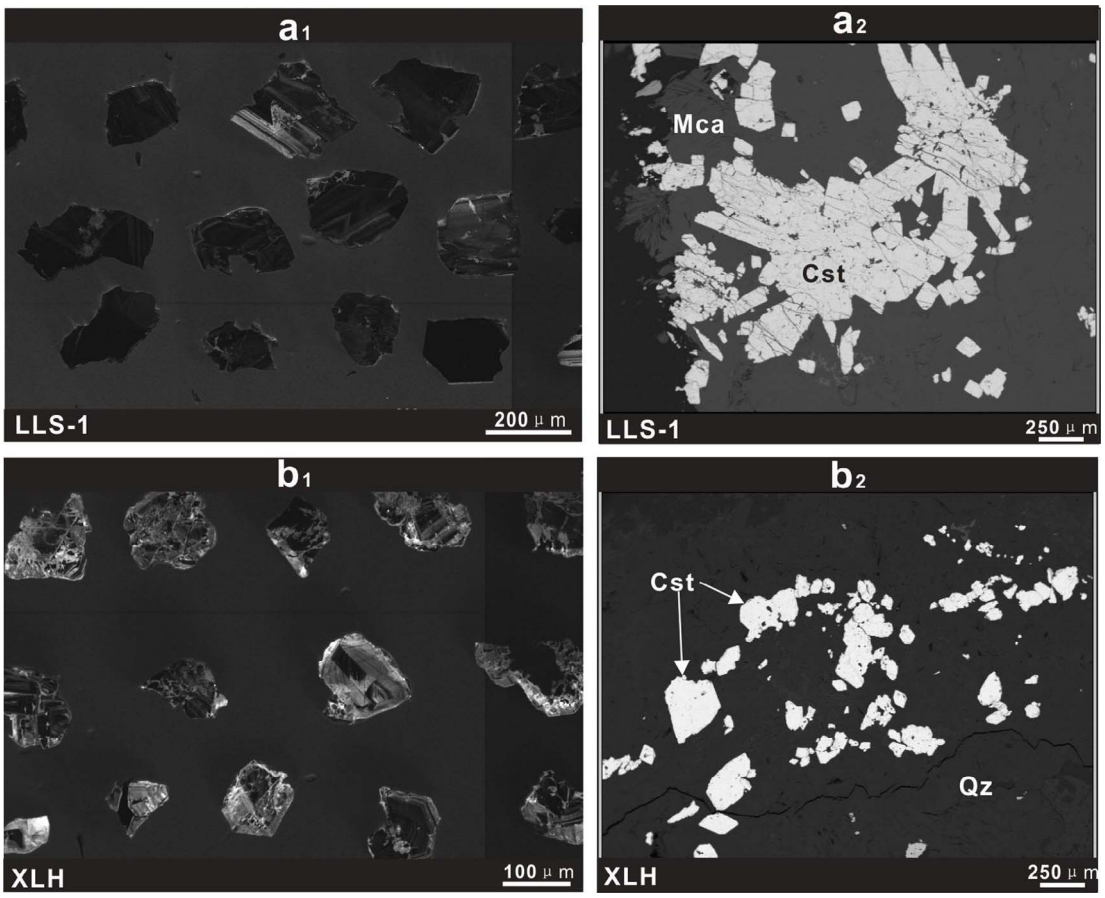

Fig. 4. Cathodoluminescence (CL) and backscattered electron (BSE) images of cassiterite grains (LLS-1 from the Lailishan tin deposit; XLH from the Xiaolonghe tin deposit). Abbreviations: Cst: cassiterite; Mca: muscovite; Qz: quartz.

for He and Ar isotopic analysis. All the samples were first crushed, and then the pyrite grains were handpicked under a binocular microscope. The pyrite grains for the He and Ar isotopic analyzes (1–2 g for each sample) were coarse-grained with no fractures, and had nearly perfect crystal habit. The pyrite grains used in the sulfur isotopic analysis were further crushed into powder and passed through a 200-mesh sieve after cleaning the powder ultrasonically and drying.

3.2. Sulfur isotopic analysis

For the sulfur isotopic analysis, we used a continuous flow isotope-ratio mass spectrometer (CF-IRMS) (EA-IsoPrime; EA: Euro 3000; IRMS: GVinstruments) at the State Key Laboratory of Environmental Geochemistry, Institute of Geochemistry, Chinese Academy of Sciences. Standards (Ag_2S) GBW 04415 ($\delta^{34}S = 22.15‰$) and GBW 04414 ($\delta^{34}S = -0.07‰$) were used for analytical quality control. The in-run precision was ± 0.2‰ (n = 5). Internal $d^{34}S_{CDT}$ (CDT: Canyon Diablo Troilite) standard samples were regularly analyzed.

3.3. He and Ar isotopic analysis

He and Ar isotopic compositions from sixteen pyrite samples were measured with an all-metal extraction line and mass spectrometer (GV 5400) at the State Key Laboratory of Ore Deposit Geochemistry, Institute of Geochemistry, Chinese Academy of Sciences. Instrument sensitivity for He and Ar was 3.9725×10^{-4} A/Torr and 1.1018×10^{-3} A/Torr, respectively. The resolution of the high-mass Faraday and electron multiplier was 228.1 and 628.3, respectively. ^{3}He and ^{4}He were collected at the electron multiplier and Faraday cup, respectively. Approximately 500–1000 mg of coarse-grained pyrite grains was loaded in vacuum crusher buckets after ultrasonic cleaning in acetone and dried. The samples were baked at 120–150 °C in the crusher buckets for ca. 24 h to remove adhered atmospheric gases, and then the crusher buckets were introduced into the high-vacuum system. Gases from the fluid inclusions were released by sequentially crushing the pyrite grains under high-vacuum conditions (10^{-8} Torr) and then loading them into the gas purification system to purify the released gases. Helium was separated from Ar using an activated charcoal cold finger at liquid N_2 temperatures (−196 °C) for 40–60 min to trap Ar. The isotope ratios and abundances of He and Ar were measured using the GV 5400 with an analytical error of < 10%. He and Ar abundances and isotopic ratios were calibrated against pipettes of 0.1 cm^3 STP air (^{4}He: 5.2×10^{-7} cm^3 STP; ^{40}Ar: 9.3×10^{-4} cm^3 STP). Procedural blanks were $< 2 \times 10^{-10}$ cm^3 STP for ^{4}He and (2–4) $\times 10^{-10}$ cm^3 STP for ^{40}Ar and constituted < 1% of the analysis. This did not affect the calibration of the measurements. The analytical procedures were similar to those described by Li et al. (2011) and Hu et al. (2012).

4. Results

4.1. Sulfur isotopes

The sulfur isotopic compositions of pyrite grains from the Lailishan and Xiaolonghe tin deposits are listed in Table 1. The $\delta^{34}S$ values of pyrite grains from the Lailishan tin deposit range from +4.9‰ to +6.7‰, with an average value of +5.53‰. The $\delta^{34}S$ values of pyrite grains from the Xiaolonghe tin deposit vary from +5.0‰ to +8.1‰, with an average value of +6.33‰. The $\delta^{34}S$ values of the four tin ore clusters (Xiaolonghe, Wandanshan, Dasongpo, and Huangjiashan) of the Xiaolonghe tin deposit were from +5.0‰ to +6.8‰, +5.1‰ to

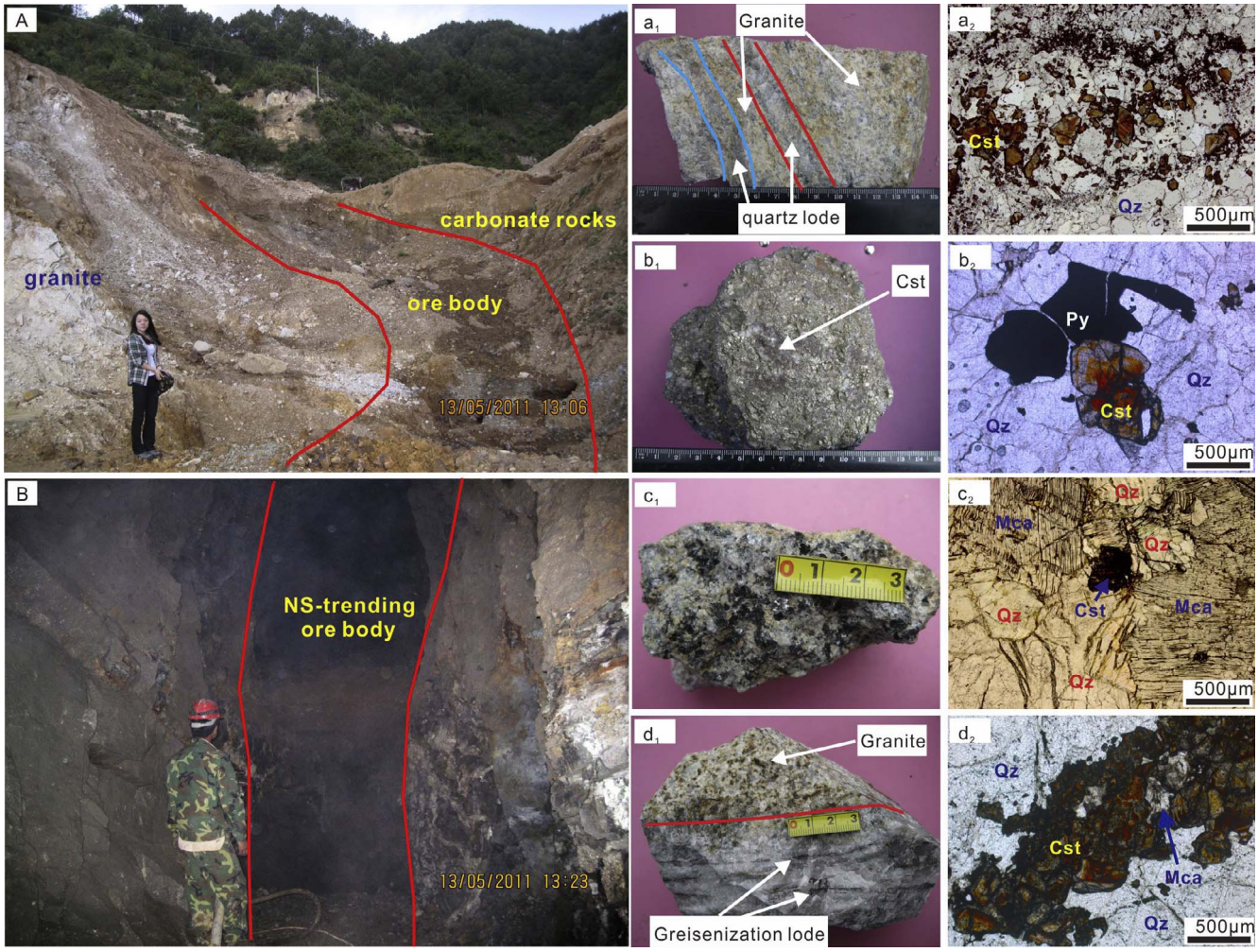

Fig. 5. Images of the ore bodies and mineral assemblages in the Xiaolonghe tin deposit. (A) The Xiaolonghe ore cluster is in the inner contact zone between the Xiaolonghe granite unit and surrounding rocks; (B) nearly N-S-trending ore body of the Dasongpo ore cluster; (a_1 and a_2) greisen vein-type ore in the interior of the Xiaolonghe granite from the Xiaolonghe ore cluster; (b_1 and b_2) quartz–sulfide-type ore from the Wandanshan ore cluster; (c_1 and c_2) greisen-type ore from the Dasongpo ore cluster and (d_1 and d_2) greisen vein-type ore from the Huangjiashan ore cluster. Abbreviations: Cst: cassiterite; Py: pyrite; Mca: muscovite; Qz: quartz.

+7.4‰, +5.4‰ to +7.0‰, and +6.5‰ to +8.1‰, respectively.

4.2. He and Ar isotopes

The measured He and Ar isotopic compositions of fluid inclusions in the pyrite grains from the Lailishan and Xiaolonghe tin deposits are listed in Table 2. The concentrations of ^{4}He and ^{40}Ar in the Lailishan tin deposit ranged from 6.56 to 27.06 × 10^{-7} cm^3 STP g^{-1} and 3.77–17.17 × 10^{-7} cm^3 STP g^{-1}, respectively. The ^{3}He/^{4}He values varied from 1.57 Ra to 3.46 Ra, with an average of 2.078 Ra, and the ^{40}Ar/^{36}Ar values ranged from 382.00 to 622.99 Ra, with an average value of 459.67 Ra.

The concentrations of ^{4}He and ^{40}Ar of the four tin ore clusters from the Xiaolonghe tin deposit were 1.86–48.18 × 10^{-7} cm^3 STP g^{-1} and 7.74–24.86 × 10^{-7} cm^3 STP g^{-1}, respectively. The ^{3}He/^{4}He values varied from 0.53 Ra to 0.88 Ra, with an average value of 0.686 Ra, and the ^{40}Ar/^{36}Ar values ranged from 301.06 to 348.43 Ra, with an average value of 322.04 Ra. In general, the ^{3}He/^{4}He and ^{40}Ar/^{36}Ar values of the Lailishan tin deposit were higher than those of the Xiaolonghe tin deposit.

5. Discussion

5.1. Sulfur isotopes of the Lailishan and Xiaolonghe tin deposits and implications

Sulfur is an important mineralizing agent in ore-forming hydrothermal systems. The sulfur sources of ore-forming fluids are inferred by the total sulfur values ($\delta^{34}S_{\Sigma S}$) (Ohmoto, 1972; Ohmoto and Rye, 1979). The sulfur isotopic composition could be affected by a change in oxygen fugacity and pH. Thus, in the absence of sulfate minerals, the pyrite $\delta^{34}S$ values are approximately equal to the total sulfur values ($\delta^{34}S_{\Sigma S}$) of ore-forming fluids (Ohmoto, 1972). Pyrite is the most common sulfide mineral in the Lailishan and Xiaolonghe tin deposits. The pyrite grains collected from these two tin deposits coexist with the cassiterite of the main metallogenic stage. Furthermore, the pyrite grains from the Lailishan and Xiaolonghe tin deposits have high Sn content, i.e., up to 1000 ppm and have the same trace elements as the cassiterite grains of the two tin deposits (Tang, 1992), suggesting a close relationship between pyrite and tin mineralization. Therefore, total sulfur values ($\delta^{34}S_{\Sigma S}$) of the ore-forming fluids of the Lailishan and Xiaolonghe tin deposits are represented by the $\delta^{34}S$ values of pyrite. From Table 1 and Fig. 6, one can see the narrow ranges of the $\delta^{34}S$ values of the pyrite grains from the Lailishan and Xiaolonghe tin deposits. This suggests that each of the two deposits originated from a

Table 1
S isotopic compositions of the pyrite samples from the Lailishan and Xiaolonghe tin deposits.

Deposit	Sampling location	Sample no.	Mineral	$\delta^{34}SV_{-CDT}$‰	Deposit	Sampling location	Sample no.	Mineral	$\delta^{34}SV_{-CDT}$‰
Lailishan	V-10 groups	V^{10}-2	Pyrite	5.5	*Xiaolonghe*	Dasongpo ore cluster	DSP-1	Pyrite	5.6
		V^{10}-3	Pyrite	6.7			DSP-2	Pyrite	6.3
		V^{10}-4	Pyrite	6.0			DSP-3	Pyrite	5.4
		V^{10}-7	Pyrite	5.4			DSP-4	Pyrite	5.6
		V^{10}-8	Pyrite	5.4			DSP-5	Pyrite	6.6
		V^{10}-10	Pyrite	4.9			DSP-6	Pyrite	6.9
		V^{10}-12	Pyrite	5.1			DSP-7	Pyrite	7.0
	V-36 groups	V_{36}-1	Pyrite	5.2			DSP-8	Pyrite	7.0
	V-57 groups	V_{57}-2	Pyrite	5.1			DSP-9	Pyrite	6.9
		V_{57}-7	Pyrite	6.0					
						Huangjiashan ore cluster	HJS-1	Pyrite	7.0
Xiaolonghe	Xiaolonghe ore cluster	XLH-1	Pyrite	5.6			HJS-2	Pyrite	6.9
		XLH-2	Pyrite	5.0			HJS-3	Pyrite	7.2
		XLH-3	Pyrite	5.7			HJS-4	Pyrite	7.1
		XLH-4	Pyrite	5.3			HJS-5	Pyrite	6.6
		XLH-5	Pyrite	6.3			HJS-6	Pyrite	6.5
		XLH-6	Pyrite	6.3			HJS-7	Pyrite	8.1
		XLH-7	Pyrite	5.9					
		XLH-8	Pyrite	5.8					
		XLH-9	Pyrite	6.2					
		XLH-10	Pyrite	6.8					
	Wandanshan ore cluster	WDS-1	Pyrite	7.4					
		WDS-2	Pyrite	5.1					
		WDS-3	Pyrite	6.4					
		WDS-4	Pyrite	5.4					
		WDS-5	Pyrite	6.3					
		WDS-6	Pyrite	6.5					

highly homogeneous sulfur source, with weak sulfur isotopic fractionation. The $\delta^{34}S$ values of the pyrite grains from the Lailishan tin deposit range from +4.9‰ to +6.7‰, with an average value of +5.53‰. The $\delta^{34}S$ values of the pyrite grains from the Xiaolonghe tin deposit varied from +5.0‰ to +8.1‰, with an average value of +6.33‰. The $\delta^{34}S$ values of the two tin deposits are slightly higher than those of the granites (0.0‰ to +5.7‰) in the Tengchong–Lianghe area (Chen et al., 1988; Shi et al., 1989), indicating mainly magmatic sources with a small amount of S from the strata involved. In addition, the Co/Ni values in the pyrite from the Lailishan tin deposit are up to 4.23 (Xu et al., 2010), which suggests a magmatic origin. Moreover, the hydrogen and oxygen isotopic data for the two tin deposits and associated granites reported in the past (Chen et al., 1988; Luo et al., 1994; Cao et al., 2016; Zhang et al., 2017) suggest that the ore-forming fluids and granite magma had clearly distinct evolutions (Fig. 7). The δD values of the Lailishan and Xiaolonghe granites gradually decreased from early to late stage, with fairly constant $\delta^{18}O$ values (Fig. 7). The $\delta^{18}O$ values of the Lailishan and Xiaolonghe tin deposits deviated with decreasing δD values (Fig. 7), suggesting a variable meteoric water contribution. Therefore, we conclude that the ore-forming fluids of the Lailishan and Xiaolonghe tin deposits originated from mixed sources of magmatic water with incremental input of meteoric water. The granitic magma provided a large proportion of the ore-forming fluids and sulfur for the Lailishan and Xiaolonghe tin deposits.

Table 2
He and Ar isotopic compositions ($\times 10^{-8}$ cm^3 STP) and isotopic ratios of inclusion-trapped fluids in pyrites from the Lailishan and Xiaolonghe tin deposits.

Deposit	Sample no.	Weight (g)	^4He	^{40}Ar	^{36}Ar	$^{40}Ar^*$	$^{40}Ar/^{36}Ar$	$^{40}Ar^*/^4He$	$^3He/^4He$ (Ra)	F^4He	$^4He_{mantle}$ (wt.%)
Lailishan tin deposit	V^{10}-2	0.19	12.31	7.07	0.0185	1.60	382.00	0.1300	3.46	3852.01	57.66
	V^{10}-3	0.21	27.54	11.00	0.0225	4.36	489.19	0.1582	1.61	7089.79	26.66
	V^{10}-4	0.22	46.40	11.49	0.0184	6.04	622.99	0.1302	1.66	14,565.71	27.51
	V^{10}-7	0.15	13.20	4.82	0.0113	1.48	426.14	0.1120	1.57	6756.02	26.00
	V^{10}-8	0.23	63.38	40.20	0.1006	10.47	399.49	0.1651	2.19	3646.84	36.34
	V^{10}-10	0.39	36.96	27.13	0.0619	8.83	438.19	0.2390	1.99	3456.55	33.02
Xiaolonghe tin deposit (comprises four ore clusters)											
Xiaolonghe ore cluster	XLH-1	0.31	5.76	17.79	0.0581	0.63	306.28	0.1086	0.88	574.57	14.44
	XLH-4	0.26	8.34	19.35	0.0643	0.36	301.06	0.0429	0.73	750.93	11.94
	XLH-5	0.31	11.17	21.25	0.0690	0.87	308.15	0.0781	0.87	937.88	14.41
Wandanshan ore cluster	WDS-2	0.22	4.07	16.97	0.0556	0.55	305.44	0.1356	0.65	424.37	10.70
	WDS-5	0.29	41.01	28.68	0.0877	2.77	327.09	0.0675	0.63	2708.04	10.33
Dasongpo ore cluster	DSP-2	0.32	44.30	21.63	0.0621	3.29	348.43	0.0742	0.63	4131.66	10.38
	DSP-3	0.33	10.28	26.31	0.0861	0.87	305.63	0.0849	0.58	691.14	9.55
	DSP-6	0.14	66.79	34.47	0.1004	4.81	343.46	0.0721	0.66	3853.86	10.88
Huangjiashan ore cluster	HJS-2	0.20	51.71	30.04	0.0871	4.29	344.77	0.0830	0.70	3436.64	11.54
	HJS-6	0.20	40.65	25.81	0.0782	2.70	330.07	0.0665	0.53	3009.93	8.60

Note: $^{40}Ar^*$ is radiogenic ^{40}Ar, given all of the Ar come from the fluid inclusions, which can be expressed as $^{40}Ar^* = {}^{40}Ar_{sample} - 295.5 \times {}^{36}Ar_{sample}$; F^4He values demonstrate enrichment of ^4He in the fluid relative to air, which can be illustrated as $F^4He = (^4He/^{36}Ar)_{sample}/(^4He/^{36}Ar)_{air}$, where $(^4He/^{36}Ar)_{air} = 0.1727$ (Stuart et al., 1995); $^4He_{mantle}$ values represent weight percent of mantle helium compared with crustal helium, which could be calculated as $^4He_{mantle}(wt.\%) = 100[(^3He/^4He)_{sample} - (^3He/^4He)_{crust}]/[(^3He/^4He)_{mantle} - (^3He/^4He)_{crust}]$, assuming a mantle R/Ra = 6.00 and crustal R/Ra = 0.01 (Anderson, 2000).

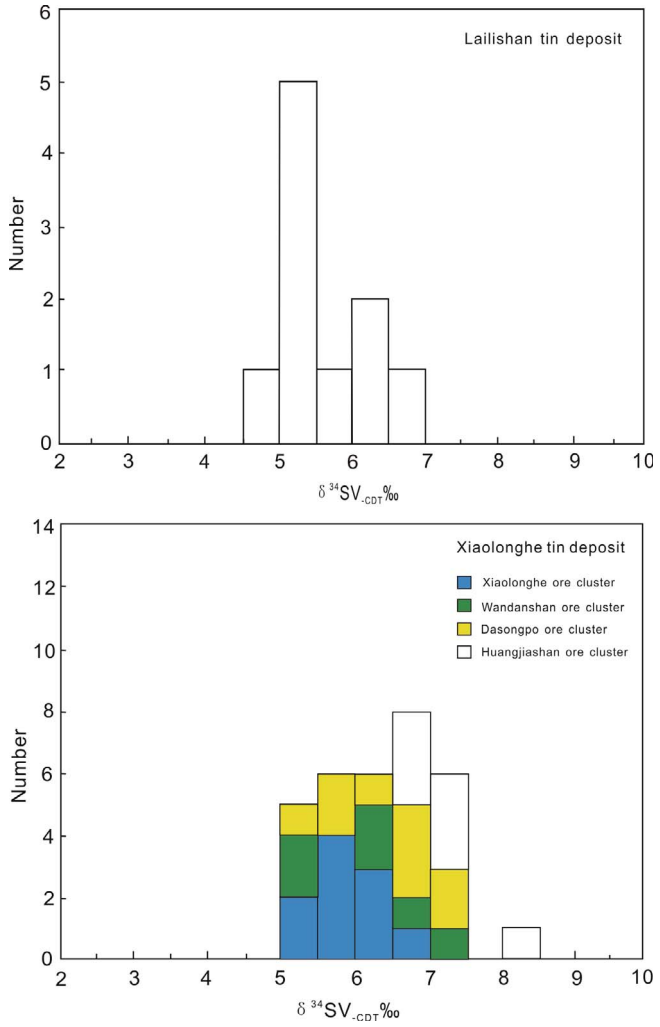

Fig. 6. $\delta^{34}S$ histogram from pyrite samples from the Lailishan and Xiaolonghe tin deposits.

5.2. He and Ar isotopes of the Lailishan and Xiaolonghe tin deposits and implications

The ore deposits have been overprinted and re-worked by later geological processes since their formation. He and Ar isotopic compositions of the fluid inclusions might be affected by late diffusion-induced loss, exogenous superposition, and isotopic fractionation (Hu et al., 2012). Nevertheless, noble gases are typically not affected by diffusion loss if they are trapped in fluid inclusions within sulfate or sulfide minerals, particularly pyrite. Pyrite is considered the best mineral for He and Ar preservation because of its extremely low He diffusivity (Stuart et al., 1994; Hu et al., 1998, 2004; Burnard et al., 1999; Sun et al., 2009; Wu et al., 2011); even the most readily diffused He compositions of inclusion-trapped fluids in pyrites are unlikely to extensively diffuse within 100 Ma (Burnard et al., 1999). Furthermore, even if the trapped He and Ar are partially lost, the values of $^{3}He/^{4}He$ and $^{40}Ar/^{36}Ar$ can remain unchanged (Baptiste and Fouquet, 1996; Hu et al., 1998, 1999, 2004; Ballentine and Burnard, 2002). Given that the Lailishan and Xiaolonghe tin deposits have mineralization ages of ca. 52 Ma and ca. 72 Ma, respectively, the diffusion loss of He and Ar is relatively limited and does not notably affect the measured He and Ar isotopic compositions. The nuclear decay of radioactive Li, U, Th, and K from host minerals or fluid inclusions can produce ^{4}He and ^{40}Ar (Stuart et al., 1995). The measured He and Ar isotopic compositions should not be affected by the nuclear decay of Li because pyrite is not an Li-bearing mineral (Ballentine and Burnard, 2002). Actually, the hydrothermal fluids usually contain very low concentrations of U and Th (Norman and Musgrave, 1994) and do not contain Th (Hu et al., 1999). The *in-situ*-produced ^{4}He from the nuclear decay of U and Th in the lattice of host pyrites cannot diffuse into the fluid inclusions after the trapping of fluid inclusions (Simmons et al., 1987; Stuart and Turner, 1992; Stuart et al., 1995). Although fluids are released from fluid inclusions by crushing of the host minerals, the ^{4}He from the nuclear decay of U and Th in the lattice of the host minerals cannot be released (Stuart and Turner, 1992). Moreover, the *in-situ*-produced ^{40}Ar from the mineral lattice or fluid inclusions are likely negligible because of the low Ar diffusivity and the extremely low K concentration in pyrite (York et al., 1982; Smith et al., 2001). Therefore, ^{4}He and ^{40}Ar produced *in situ* by the nuclear decay of radioactive elements in the host minerals or fluid inclusions does not affect the initial He and Ar isotopic compositions of fluid inclusions in pyrite. Noble gases from secondary fluid inclusions may be easily mistaken as noble gases from primary fluid inclusions. To avoid this, all the pyrite grains in this study have perfect crystal morphology and are coarse-grained, with no cracks. In addition, the pyrite samples were all collected from underground mines, which minimizes the effect of cosmogenic ^{3}He (Simmons et al., 1987; Stuart et al., 1995). Therefore, the measured He and Ar isotopic compositions could represent the ore-forming fluids of the Lailishan and Xiaolonghe tin deposits.

Noble gases in crustal fluids have three potential sources with extremely variable isotopic signatures that include the following: air-saturated rainwater, mantle-derived fluids, and crust-derived fluids (Turner et al., 1993a,b; Stuart et al., 1995; Burnard et al.,1999). Air-saturated water (meteoric water or seawater) has He and Ar isotopic compositions of $^{3}He/^{4}He = 1$ Ra ($1\ Ra = 1.39 \times 10^{-6}$) and $^{40}Ar/^{36}Ar = 295.5$ Ra (Turner et al., 1993a,b; Stuart et al., 1995; Burnard et al., 1999). Atmospherically derived He is unlikely to affect He abundance and the isotopic compositions of most crustal fluids owing to the insolubility of He in water and the low He concentration in the atmosphere (Stuart et al., 1994; Ozima and Podosek, 2001). Therefore, the mantle and the crust sources of He probably contributed to the He isotopic compositions in the ore-forming fluids. The He isotopic compositions in the mantle have $^{3}He/^{4}He$ values of 6–7 Ra, whereas the corresponding Ar isotopic compositions are mainly radiogenic Ar with large variations in the $^{40}Ar/^{36}Ar$ values (> 40,000). The isotopic compositions of He and Ar in the crust-derived fluids are mostly radiogenic He and Ar with $^{3}He/^{4}He = 0.01–0.05$ Ra and $^{40}Ar/^{36}Ar > 45{,}000$ Ra (Turner et al., 1993a,b; Dunai and Baur, 1995; Stuart et al., 1995; Burnard et al., 1999). This large difference in isotopic ratios makes the crust and the mantle contributions to ore formation traceable by He and Ar isotopes from fluid inclusions in pyrite.

The $^{3}He/^{4}He$ values of the Lailishan (1.57–3.46 Ra) and Xiaolonghe tin deposits (0.53–0.88 Ra) are obviously higher than those of the He produced in the continental crust but lower than those of the mantle, demonstrating that both mantle- and crustal-derived He is present at different proportions in the ore-forming fluids of the two tin deposits (Table 2). In the $^{3}He/^{36}Ar$ vs $^{40}Ar/^{36}Ar$ (Fig. 8a) and $^{40}Ar/^{36}Ar$ vs $^{3}He/^{4}He$ (Fig. 8b) plots, the pyrite samples from the Lailishan and Xiaolonghe tin deposits plot in the area between the mantle and crustal end members. Moreover, in the ^{3}He vs ^{4}He (Fig. 8c) and $^{3}He/^{4}He$ vs $^{40}Ar*/^{4}He$ (Fig. 8d) plots, the noble gas isotopic data show clear mixing between crustal- and mantle-derived components, which confirms the variable contributions of mantle He to the Lailishan and Xiaolonghe tin deposits hydrothermal system. Given the simple, separate binary mixing of the crustal and mantle components, the proportions of mantle ^{4}He could be calculated according to $^{4}He_{mantle}$ (%) = $100 \times [(^{3}He/^{4}He)_{sample} - (^{3}He/^{4}He)_{crust}]/[(^{3}He/^{4}He)_{mantle} - (^{3}He/^{4}He)_{crust}]$, assuming a mantle R/Ra of 6.00 and a crustal R/Ra of 0.01 (Anderson, 2000). The mantle ^{4}He values of the Lailihsan tin deposit range from 26% to 44%, whereas these values of the Xiaolonghe tin deposit range from 8% to 15% (Table 2). As previously mentioned, the ore-forming fluids of the Lailishan and

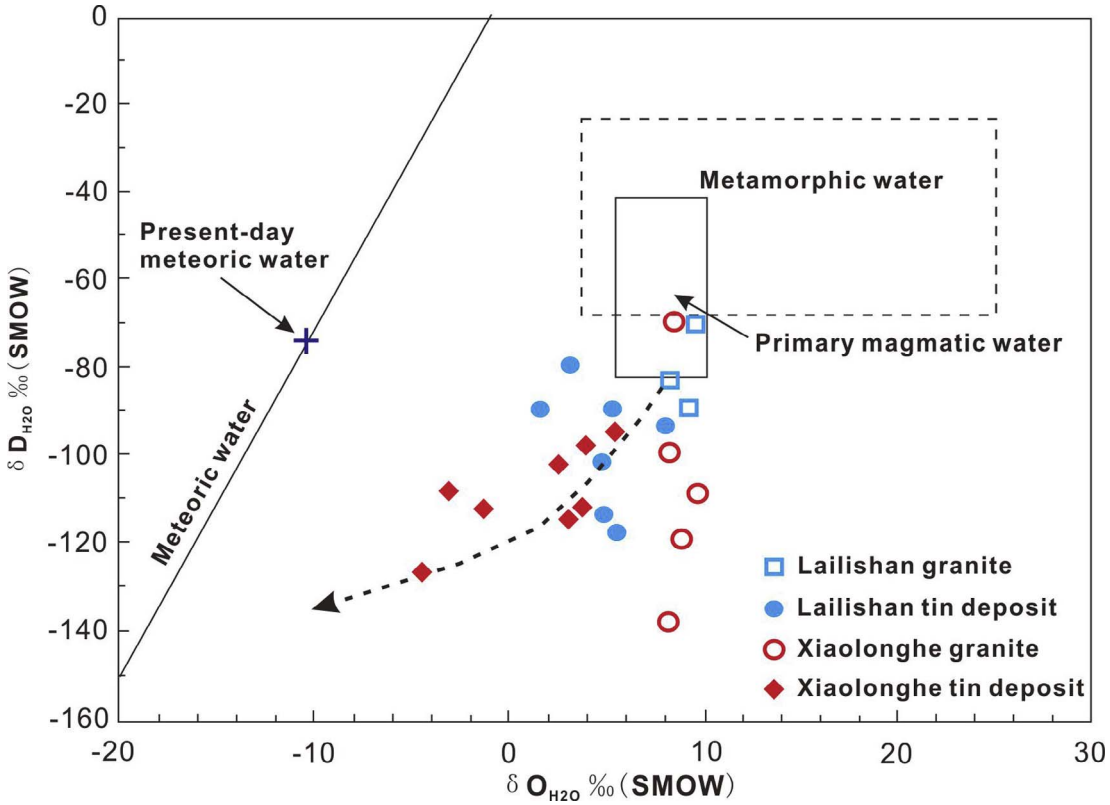

Fig. 7. Hydrogen versus oxygen isotope compositions in the Lailishan and Xiaolonghe tin deposits (modified from Taylor (1974)). The hydrogen and oxygen isotopic compositions of the Lailishan and Xiaolonghe granites are from Chen et al. (1988) and Luo et al. (1994); the data for the Lailishan tin deposit are from Zhang et al. (2017), and the data for the Xiaolonghe tin deposit are from Cao et al. (2016).

Xiaolonghe tin deposits were dominantly derived from granitic magmas. Thus, we infer that the mixture of mantle and crustal He are magmatic contributions. Deep mantle-derived He should be involved in the ore-forming fluids through granitic magmatism. Both the $^{40}Ar/^{36}Ar$ values and the positive correlation of $^{3}He/^{36}Ar$ and $^{40}Ar/^{36}Ar$ (Fig. 8a) of the two deposits reflect the dilution of magmatic fluids by meteoric fluids in the hydrothermal system. The intercept of the best-fit line in Fig. 8a identifies a $^{40}Ar/^{36}Ar$ value of 355 Ra for the crustal fluid component, which is higher than that of atmospheric Ar ($^{40}Ar/^{36}Ar$ = 295.5 Ra), and represents the meteoric fluid component within a small volume of crustal radiogenic ^{40}Ar. This might have been caused by crustal radiogenic ^{40}Ar mixed in the meteoric fluids when meteoric water participated in the underground cycle.

5.3. The relationship between A-type granites and tin deposits

Tin mineralization is traditionally considered to be associated with granites that are enriched in Sn, F, B, Li, and Cs. In general, these are highly fractionated S-type or ilmenite-series granites (Heinrich, 1990; Stemprok, 1990; Taylor and Wall, 1993). Magmatic differentiation can produce voluminous Sn-enriched ore-forming fluids during their evolution (Taylor and Wall, 1993). Recently, an increasing number of studies (Bettencourt et al., 2005; Haapala and Lukkari, 2005; Li et al., 2006; Jiang et al., 2006, 2008; Bi et al., 2008; Chen et al., 2015; Jiang et al., 2017) have emphasized the relationship between A-type granites and tin mineralization, which offers new perspectives on Sn metallogenesis. A-type granites were first described as anhydrous granitic rocks with high alkaline content in anorogenic settings (Loiselle and Wones, 1979). The classification of I-, S-, and A-type granites is sometimes difficult, particularly for highly fractionated rocks (Chappell and White, 1992; King et al., 2001; Bonin, 2007; Wu et al., 2007). Although there is still much debate on the origin of A-type granites, their unique mineralogical and geochemical characteristics are widely recognized. A-type granites have high SiO_2, K_2O, Fe/Mg, and incompatible elements, such as REE (except Eu), Zr, and Hf, but are low in Al_2O_3, CaO, Ba, Sr, and Eu contents (Collins et al., 1982). They are enriched in high field-strength element contents (Zr + Nb + Ce + Y > 350 ppm) and high Ga/Al (10,000 × Ga/Al > 2.6) (Whalen et al., 1987). S-type granites commonly belong to the calc-alkaline series with ASI > 1.1 and contain Al-rich silicate minerals such as muscovite, garnet, and cordierite (Clemens, 2003; Ishihara, 2007; Chappell and Wyborn, 2012). In contrast, A-type granitic rocks belong to the alkaline and peralkaline series and contain Fe–Mg silicate minerals such as Fe-rich biotite and amphibole (Bonin, 2007). A-type granites are commonly richer in alkaline and HFSE elements (Zr, Nb, Y, REE, and Ga) compared to I-type granites. In addition, it is commonly considered that A-type granites are formed by anhydrous and high-temperature felsic rocks (Clemens et al., 1986; Patiño Douce, 1997). The Lailishan and Xiaolonghe granitoids are dominantly biotite-bearing granites. They are weakly peraluminous to metaluminous with A/CNK values < 1.1 and are silica (SiO_2 = 73.3–76.2 wt%) and alkali rich ($K_2O + Na_2O$ = 8.32–9.17 wt %). They have high zircon saturation temperatures (774–833 °C), high Zr + Nb + Ce + Y contents (272–416 ppm), and high 10,000 × Ga/Al (2.02–3.52). Furthermore, these granites have high total REE contents (174–404 ppm) and significant negative Eu anomalies. These mineralogical and geochemical signatures are clearly characteristic of A-type granites. The details of the Lailishan and Xiaolonghe granitoids were discussed in a previous study (Chen et al., 2015).

We have successively argued that mineralization in the Lailishan and Xiaolonghe tin deposits is contemporaneous with the emplacement of the A-type granites (Chen et al., 2014; Chen et al., 2015), which strongly supports an intrusion-related origin for the two deposits. As previously demonstrated, the hydrogen, oxygen, and sulfur isotopic compositions of the Lailishan and Xiaolonghe tin deposits in the Tengchong–Lianghe tin belt suggest that the ore-forming fluids and sulfur were principally derived from the granitic magma, which

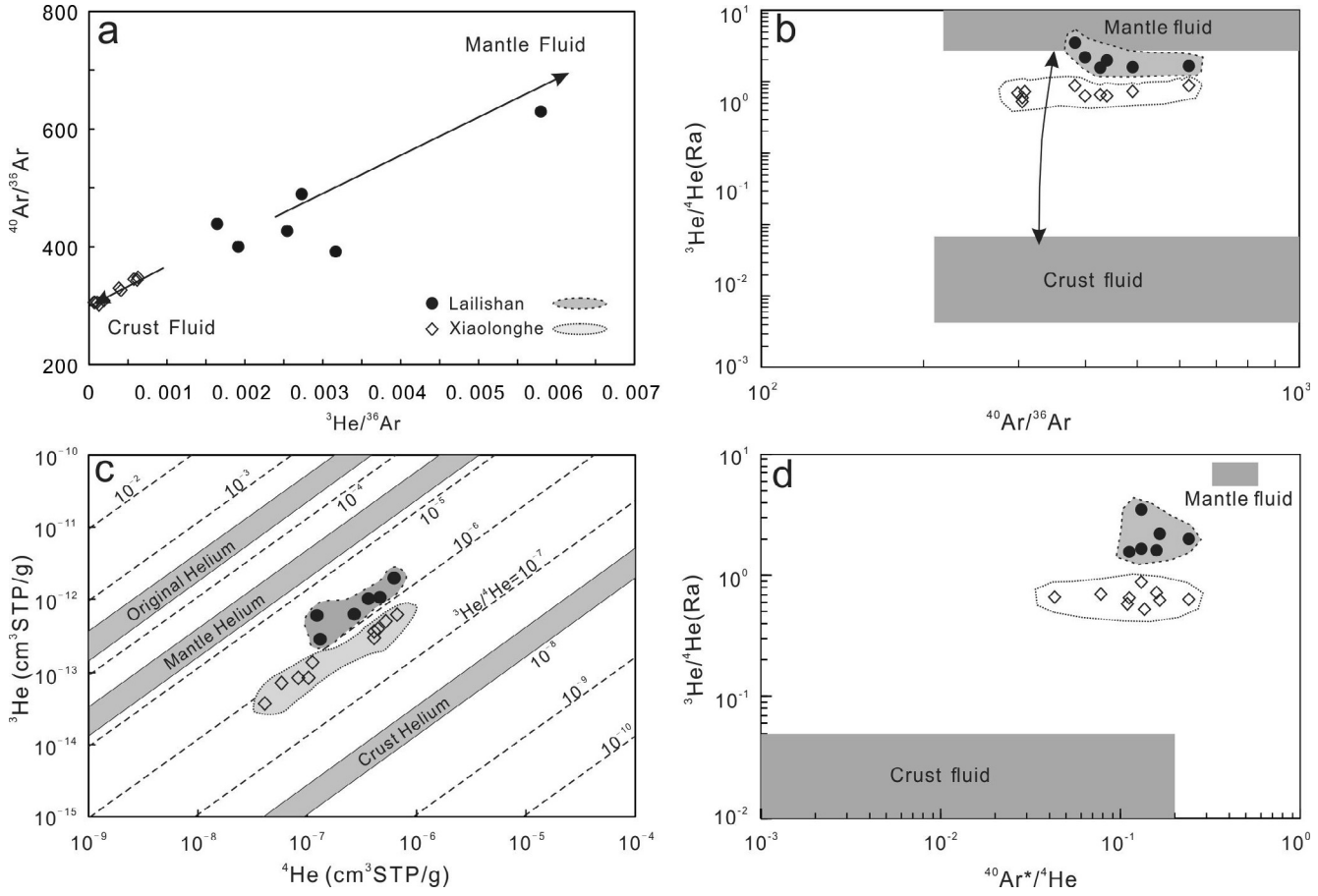

Fig. 8. (a) $^{40}Ar/^{36}Ar$ vs $^{3}He/^{36}Ar$, (b) $^{40}Ar/^{36}Ar$ vs $^{3}He/^{4}He$, (c) ^{4}He vs ^{3}He and (d) $^{40}Ar^{*}/^{4}He$ vs $^{3}He/^{4}He$ plots of inclusion-trapped fluids in pyrites from the Lailishan and Xiaolonghe tin deposits.

confirms the close relationship between the granites and tin deposits. The He and Ar isotope compositions further prove that the ore-forming fluids of the two deposits are mainly magmatic with different amounts of meteoric water. Actually, granites not only provided the ore-forming fluids for the Lailishan and Xiaolonghe tin deposits but also significantly contributed to the Sn enrichment. The Lailishan and Xiaolonghe granites have relatively high Sn contents with an average value of 15.2 ppm (Chen et al., 2015), which is clearly higher than the average crustal values (2–3 ppm). The high Sn contents of the granites apparently originate from source rocks with abundant Sn. In a previous study (Chen et al., 2015) of the Lailishan and Xiaolonghe granites, we argued that these granites were derived from high-temperature melting of Paleo- to Neo-Proterozoic mafic and metasedimentary basement with high Sn contents (average value of 10 ppm) (Mao et al., 1987). Therefore, granitic magmas with high Sn content are crucial for the tin mineralization of the Lailishan and Xiaolonghe tin deposits in the Tengchong–Lianghe tin belt. These tin deposits should be certainly classified as magmatic hydrothermal deposits. In addition, the ore-hosting strata in the Tengchong–Lianghe area are also Sn-enriched (32–48 ppm) (Zhang, 1986). Thus, we propose that deep-seated granitic magmas with mantle He ascended and intruded into the stress-relaxed region. Sn is an incompatible element, which tends to enter the melt phase during magmatic differentiation. Ore-forming fluids with high Sn contents and mantle He and S were produced by magmatic differentiation during the A-type granitic magmatism. When the ore-forming fluids invaded the country rocks, Sn, S, and meteoric Ar from the surrounding strata mixed with the fluids. Ore-forming Sn was released from the magma and the surrounding strata owing to hydrothermal alteration and was then deposited in favorable places such as the fracture zones between the granitic plutons and the wall rocks (the ore bodies of the Lailishan tin deposit mostly occur in the contact zone between the Lailishan granitic pluton and the surrounding rocks) or the interior of the granite (the ore bodies of the Xiaolonghe tin deposit mostly occurred at the top or edge of the Xiaolonghe granite).

5.4. Differences in the He and Ar isotopic compositions between the Lailishan and Xiaolonghe tin deposits and implications for the tectonic environment

High $^{3}He/^{4}He$ values (6–7 Ra) are characteristics of mantle-derived fluids (Turner et al., 1993a,b; Stuart et al., 1995), which makes the mantle the only plausible source of the end-member with high $^{3}He/^{4}He$. The $^{3}He/^{4}He$ values (0.53–3.46 Ra) of the ore-forming fluids of the Lailishan and Xiaolonghe tin deposits are obviously higher than those of the crust ($^{3}He/^{4}He$ = 0.01–0.05 Ra), suggesting different proportions of mantle-derived fluids in the ore-forming fluids of the two deposits. As previously mentioned, the mantle ^{4}He values of the Lailihsan deposit range from 26% to 44%, whereas values of the Xiaolonghe deposit range from 8% to 15% (Table 2). The $^{3}He/^{4}He$ values of the Lailishan deposit (1.57–3.46 Ra) are obviously higher than those of the Xiaolonghe deposit (0.53–0.88 Ra) (Table 2). In addition, in the He–Ar-related plots (Fig. 8), the pyrite samples from the Lailishan tin deposits plot closer to the mantle endmembers. These data suggest that there are more contributions of mantle-derived fluids to the ore-forming fluids of the Lailishan tin deposit relative to the Xiaolonghe tin deposit. The magmatic volatiles could mix with the hydrothermal system because the transport of fluids from the magma into the hydrothermal system cannot significantly induce fractionation of He and Ar (Graham, 2002; Hu et al., 2004). The aforementioned results suggest that deep mantle-derived He should have been involved in the ore-forming fluids of the

Lailishan and Xiaolonghe tin deposits. The magmatism in the Tengchong–Lianghe area is characterized by S-, I-, and A-type granitoids with emplacement ages ranging from the Early Cretaceous to Late Cretaceous and Early Cenozoic (Chen et al., 1987; Hou et al., 2007; Jiang et al., 2012; Xu et al., 2012; Chen et al., 2015). Their emplacement ages decrease obliquely to the regional geological strike from NE to SW. The Hf and O isotopic compositions of these granitic plutons also delineate an E–W variation, with $\varepsilon Hf_{(t)}$ values increasing progressively and $\delta^{18}O$ values gradually decreasing from east to west (Xu et al., 2012; Chen et al., 2015), indicating more mantle contribution to the magmatism during the young stages. The spatial variation in the magmatism of the Tengchong–Lianghe area is comparable to that in Tibet, in which a number of granitoids are present and range in age from Jurassic to Paleogene (Hou et al., 2006; Ji et al., 2009a,b; Wen et al., 2008). In the Tibetan Plateau, the most characteristic granites are exposed along the southern margin of the Lhasa terrane and extend from the Kohistan–Ladakh batholith in the west through the Gangdese batholith in the central area to the Chayu–western Yunnan–Burma batholith in the east (Ji et al., 2009a). Thus, the Tengchong–Lianghe granite belt has been considered as the eastern segment of the Gangdese magmatic arc (Hou et al., 2007; Ji et al., 2009b). The magmatism in the Gangdese magmatic arc is characterized by I-type granitoids in the south (Chu et al., 2006; Wen et al., 2008; Ji et al., 2009b), S-type granitoids in the north (Harris et al., 1990; Chung et al., 2005; Kapp et al., 2005), and some A-type granitoids in the east (Qu et al., 2002, 2012; Lin et al., 2012). Overall, the emplacement ages and Hf isotopic compositions of these granites show a N-S variation, with decreasing emplacement ages and increasing $\varepsilon Hf_{(t)}$ values (Wen et al., 2008; Ji et al., 2009a). The spatial variations in the emplacement ages and isotopic compositions of granitoids in the Tengchong–Lianghe area and Tibet also suggest that the mantle source was significantly intensive during the younger stages. The magmatism in Tibet is presumably related to the Tethyan subduction during the tectonic evolution of the Lhasa terrane (Allegrè et al., 1984; Chung et al., 2005). The different proportions of mantle-derived fluids in the ore-forming fluids of the Lailishan and Xiaolonghe tin deposits may be due to the different stages of Neo-Tethyan subduction.

Mantle-derived ^{3}He in crustal fluids is generally released during intrusion of subsurface mantle-derived melts in crustal extensional settings (Oxburgh et al., 1986; Ballentine and Burnard, 2002; Hu et al., 2004). A-type granites in orogenic zones around the world were largely emplaced during lithospheric extension after continent–continent collision (Wu et al., 2002; Bonin, 2007; Zhao et al., 2008; Goodenough et al., 2010; Qu et al., 2012; Zhao et al., 2013). Recent studies have argued that the subduction of the Neo-Tethyan plate started during the Early Cretaceous and lasted until the Paleogene; the collision between the Tengchong and Baoshan blocks started after the closure of the Bangong–Nujiang Tethyan Ocean during the Late Jurassic and Early Cretaceous and the collision lasted until the Late Cretaceous (Zhu et al., 2011; Zhu et al., 2013b). The Late Cretaceous Xiaolonghe granitoids were probably associated with the subduction of the Neo-Tethyan plate under the post-collisional extension of the Tengchong and Baoshan microplates during the Jurassic–Cretaceous, while the Paleogene Lailishan granitoids might be a syncollisional product of the stretching relaxation during the middle- and late-main collisional period (55–41 Ma) between India and Asia (Chen et al., 2015). During the main collisional period (65–41 Ma) of India–Asia, the slab rollback of a flat subducted Neo-Tethyan ocean (Chung et al., 2005) was substituted by the deep subduction of the Indian continental lithosphere and the break-off of the Neo-Tethyan slab at depth (Hou et al., 2006; Mo et al., 2007). Shoshonitic dikes were discovered in the Linzhou Basin of Tibet with emplacement ages of ca. 52.9 Ma, suggesting that the magmas originated from a metasomatically enriched mantle source with some involvement of asthenospheric mantle (Yue and Ding, 2009). This suggests that asthenosphere upwelled through the “break-off window” of the Neo-Tethyan slab and triggered partial melting of the lithospheric mantle. This may explain the increased crust–mantle interaction during the Paleogene (the period wherein the Lailishan tin deposit formed) relative to the Late Cretaceous when the Xiaolonghe tin deposit formed). In addition, basic rocks and granitoids containing mafic microgranular xenoliths, emplaced from 40 to 54 Ma, are widely exposed in the Tengchong–Lianghe–Yingjiang district (Yang et al., 2009; Xu et al., 2012), which further proves the increased crust–mantle interaction during the Paleogene in western Yunnan.

6. Conclusions

The $\delta^{34}S$ values (+5.0‰ to +8.1‰) of the Lailishan and Xiaolonghe tin deposits in the Tengchong–Lianghe tin belt are slightly higher than those of the granites (0.0% to +5.7‰) in the Tengchong–Lianghe area, indicating mainly magmatic sources for the sulfur of the ore-forming fluids mixed with a small amount of S from the surrounding strata.

The He and Ar isotopic compositions of the ore-forming fluids of the Lailishan and Xiaolonghe tin deposits suggest derivation from mixed crustal and mantle sources and a small volume of meteoric sources in different proportions.

The mantle ^{4}He values and $^{3}He/^{4}He$ values of the Lailihsan tin deposit (26–44%; 1.57–3.46 Ra) are markedly higher than those of the Xiaolonghe tin deposit (8–15%; 0.53–0.88 Ra), suggesting an increased crust–mantle interaction during the Paleogene relative to the Late Cretaceous in western Yunnan.

Acknowledgments

This work was financially supported by The National Natural Science Foundation of China – China (4160020815); the 12th Five-Year Plan Project of the State Key Laboratory of Ore Deposit Geochemistry, Chinese Academy of Sciences – China (SKLODG-ZY125-03); the Startup Projects for High-level Talents of the Guizhou Institute of Technology – China (XJGC20161229); the Joint Fund of the Science and Technology Department of Guizhou Province – China (LH[2014]7358); and the Startup Projects of High-level Talents of Guizhou Institute of Technology – China (XJGC20131204). Yunnan Tin Industry Co. Ltd. is gratefully acknowledged for their kind help during field work.

References

Aitchison, J.C., Ali, J.R., Davis, A.M., 2007. When and Where Did India and Asia Collide? Geophys. Res. Solid Earth 112.
Allegrè, C.J., Courtillot, V., Tapponnier, P., Him, A., Mattauer, M., Coulon, C., Jaeger, J.J., Achache, J., Scharer, U., Marcoux, J., Burg, J.P., 1984. Structure and evolution of the Himalaya-Tibet orogenic belt. Nature 307, 17–22.
Anderson, D.L., 2000. The statistics and distribution of helium in the mantle. Int. Geol. Rev. 42, 289–311.
Ballentine, C.J., Burnard, P.G., 2002. Production, release and transport of noble gases in the continental crust. Rev. Mineral. Geochem. 47, 481–538.
Baptiste, P.J., Fouquet, Y., 1996. Abundance and isotopic composition of helium in hydrothermal sulfides from the East Pacific Rise at 13 N. Geochim. Cosmochim. Acta 60, 87–93.
Bettencourt, J.S., Leite Jr, W.B., Goraieb, C.L., Sparrenberger, I., Bello, R.M.S., Payolla, B.L., 2005. Sn-polymetallic greisen-type deposits associated with late-stage rapakivi granites, Brazil: fluid inclusion and stable isotope characteristics. Lithos 80, 363–386.
Bi, C.S., Sheng, X.Y., Xu, Q.S., 1992. New discovery of tin deposit related with Hercynian A-type granite in China. Sci. China Earth Sci. 632–638 (in Chinese with English abstract).
Bi, X.W., Li, H.L., Shuang, Y., Hu, X.Y., Hu, R.Z., Peng, J.T., 2008. Geochemical characteristics of fluid inclusions from Qitianling A-type granite, Hunan Province, China: tracing the source of ore forming fluid of the Furong superlarge tin deposit. Geol. J. China Univers. 14, 539–548 (in Chinese with English abstract).
Bonin, B., 2007. A-type granites and related rocks: evolution of a concept, problems and prospects. Lithos 97, 1–29.
Bortolotti, V., Principi, G., 2005. Tethyan ophiolites and Pangea break- up. Isl. Arc 14, 442–470.
Botelho, N.F., Moura, M.A., 1998. Granite-ore deposit relationships in Central Brazil. J. South Am. Earth Sci. 11, 427–438.
Burchfiel, B.C., Chen, Z.L., 2012. Tectonics of the Southeastern Tibetan Plateau and its adjacent foreland. Geol. Soc. Am. Mem. 210, 1–164.
Burnard, P., 2012. The Noble gases as geochemical tracers. Advances in Isotope Geochemistry. Springer, pp. 1–403.

Burnard, P.G., Hu, R.Z., Turner, G., Bi, X.W., 1999. Mantle, crustal and atmospheric noble gases in Ailaoshan gold deposits, Yunnan province. China. Geochim. Cosmochim. Acta 63, 1595–1604.
Cao, H.W., Zou, H., Zhang, Y.H., Zhang, S.T., Zheng, L., Zhang, L.K., Tang, L., Pei, Q.M., 2016. Late Cretaceous magmatism and related metallogeny in the Tengchong area: evidence from geochronological, isotopic and geochemical data from the Xiaolonghe Sn deposit, western Yunnan, China. Ore Geol. Rev. 78, 196–212.
Chappell, B.W., White, A.J.R., 1992. I-type and S-type granites in the Lachlan fold belt. Earth Environ. Sci. Trans. R. Soc. Edinb. 83, 1–26.
Chappell, B.W., Wyborn, D., 2012. Origin of enclaves in S-type granites of the Lachlan Fold Belt. Lithos 154, 235–247.
Chen, J.C., 1987. Chronology and emplacement ages of the granitic rocks in the western Yunnan. Yunnan Geol. 101–113 (in Chinese with English abstract).
Chen, J.C., Shi, L., Lin, W.X., 1988. The criteria and discrimination features of tin-bearing granite, West Yunnan. Miner. Res. Geol. 1, 22–31 (in Chinese with English abstract).
Chen, X.C., Hu, R.Z., Bi, X.W., Li, H.M., Lan, J.B., Zhao, C.H., Zhu, J.J., 2014. Cassiterite LA-MC-ICP-MS U/Pb and muscovite $^{40}Ar/^{39}Ar$ dating of tin deposits in the Tengchong-Lianghe tin district, NW Yunnan, China. Mineral. Deposita 49, 843–860.
Chen, X.C., Hu, R.Z., Bi, X.W., Zhong, H., Lan, J.B., Zhao, C.H., Zhu, J.J., 2015. Petrogenesis of metaluminous A-type granitoids in the Tengchong-Lianghe tin belt of southwestern China: evidences from zircon U-Pb ages and Hf-O isotopes, and whole-rock Sr-Nd isotopes. Lithos 93–110.
Chu, M.F., Chung, S.L., Song, B., Liu, D.Y., O'Reilly, S.Y., Pearson, N.J., 2006. Zircon U-Pb and Hf isotope constraints on the Mesozoic tectonics and crustal evolution of southern Tibet. Geology 34, 745–748.
Chung, S.L., Chu, M.F., Zhang, Y.Q., Xie, Y.W., Lo, C.H., Lee, T.Y., Lan, C.Y., Li, X.H., Zhang, Q., Wang, Y.Z., 2005. Tibetan tectonic evolution inferred from spatial and temporal variations in post-collisional magmatism. Earth-Sci. Rev. 68, 173–196.
Clarke, M.C.G., Beddoe-Stephens, B., 1987. Geochemistry, mineralogy and plate tectonic setting of a Late Cretaceous Sn-W granite from Sumatra, Indonesia. Mineral. Mag. 51, 371–387.
Clemens, J.D., 2003. S-type granitic magmas-petrogenetic issues, models and evidence. Earth-Sci. Rev. 61, 1–18.
Clemens, J.D., Holloway, J.R., White, A.J.R., 1986. Origin of an A-type granite: experimental constraints. Am. Mineral. 71, 317–324.
Collins, W.J., Beams, S.D., White, A.J.R., Chappell, B.W., 1982. Nature and origin of A-type granites with particular reference to southeastern Australia. Contrib. Mineral. Petrol. 80, 189–200.
Cong, B.L., Wu, G.Y., Zhang, Q., Zhang, R.Y., Zhai, M.G., Zhao, D.S., Zhang, W.H., 1993. Petro-tectonic evolution of the Palaeo-Tethys in the west Yunnan, China. Sci. China Earth Sci. 23, 1201–1207 (in Chinese with English abstract).
Cong, F., Lin, S.L., Xie, T., Li, Z.H., Zou, G.F., Liang, T., 2010. Rare earth element geochemistry and U-Pb age of zircons from granites in Tengchong-Lianghe area, Western Yunnan. J. Jilin Univ.: Earth Sci. Ed. 40, 573–580 (in Chinese with English abstract).
Dunai, T.J., Baur, H., 1995. Helium, neon and argon systematics of the European sub-continental mantle: implications for its geochemical evolution. Geochim. Cosmochim. Acta 59, 2767–2784.
Gonevchuk, V.G., Gonevchuk, G.A., Korostelev, P.G., Semenyak, B.I., Seltmann, R., 2010. Tin deposits of the Sikhote-Alin and adjacent areas (Russian Far East) and their magmatic association. Aust. J. Earth Sci. 57, 777–802.
Goodenough, K.M., Thomas, R.J., De Waele, B., Key, R.M., Schofield, D.I., Bauer, W., Tucker, R.D., Rafahatelo, J.M., Rabarimanana, M., Ralison, A.V., Randriamananjara, T., 2010. Post-collisional magmatism in the central East African Orogen: the Maevarano Suite of north Madagascar. Lithos 116, 18–34.
Graham, D.W., 2002. Noble gas isotope geochemistry of mid-ocean ridge and ocean island basalts: characterization of mantle source reservoirs. Rev. Mineral. Geochem. 47, 247–317.
Haapala, I., Lukkari, S., 2005. Petrological and geochemical evolution of the Kymi stock, a topaz granite cupola within the Wiborg rapakivi batholith, Finland. Lithos 80, 347–362.
Harris, N.B.W., Inger, S., Xu, R.H., 1990. Cretaceous plutonism in Central Tibet-An example of postcollision magmatism. J. Volcanol. Geoth. Res. 44, 21–32.
Heinrich, C.A., 1990. The chemistry of hydrothermal tin(-tungsten) ore deposition. Econ. Geol. 85, 457–481.
Hou, Z.Q., Mo, X.X., Gao, Y.F., Yang, Z.M., Dong, G.C., Ding, L., 2006. Early Processes and tectonic model for the Indian-Asian continental collision: evidence from the Cenozoic Gangdese Igneous Rocks in Tibet. Acta Geol. Sin. 80, 1233–1248 (in Chinese with English abstract).
Hou, Z.Q., Zaw, K., Pan, G.T., Mo, X.X., Xu, Q., Hu, Y.Z., Li, X.Z., 2007. Sanjiang Tethyan metallogenesis in SW China: tectonic setting, metallogenic epochs and deposit types. Ore Geol. Rev. 31, 48–87.
Hu, R.Z., Burnard, P.G., Turner, G., Bi, X.W., 1998. Helium and Argon isotope systematics in fluid inclusions of Machangqing copper deposit in west Yunnan province, China. Chem. Geol. 146, 55–63.
Hu, R.Z., Bi, X.W., Turner, G., Burnard, P.G., 1999. He and Ar isotopic geochemistry of the ore-forming fluids of the Ailaoshan Au ore belt. Sci. China Earth Sci. 29, 321–330 (in Chinese with English abstract).
Hu, R.Z., Burnard, P.G., Bi, X.W., Zhou, M.F., Pen, J.T., Su, W.C., Wu, K.X., 2004. Helium and argon isotope geochemistry of alkaline intrusion-associated gold and copper deposits along the Red River-Jinshajiang fault belt, SW China. Chem. Geol. 203, 305–317.
Hu, R.Z., Burnard, P.G., Bi, X.W., Zhou, M.F., Peng, J.T., Su, W.C., Zhao, J.H., 2009. Mantle-derived gaseous components in ore-forming fluids of the Xiangshan uranium deposit, Jiangxi province, China: evidence from He, Ar and C isotopes. Chem. Geol. 266, 86–95.
Hu, R.Z., Bi, X.W., Jiang, G.H., Chen, H.W., Peng, J.T., Qi, Y.Q., Wu, L.Y., Wei, W.F., 2012. Mantle-derived noble gases in ore-forming fluids of the granite-related Yaogangxian tungsten deposit, Southeastern China. Mineral. Deposita 47, 623–632.
Ishihara, S., 2007. Origin of the Cenozoic-Mesozoic magnetite-series and ilmenite-series granitoids in East Asia. Gondwana Res. 11, 247–260.
Janecka, J., Stemprok, M., 1967. Endogenous tin mineralization in the Bohemian massif. A Technical Conference on Tin, London, pp. 245–266.
Ji, W.Q., Wu, F.Y., Chung, S.L., Li, J.X., Liu, C.Z., 2009a. Zircon U-Pb geochronology and Hf isotopic constraints on petrogenesis of the Gangdese batholith, southern Tibet. Chem. Geol. 262, 229–245.
Ji, W.Q., Wu, F.Y., Liu, C.Z., Chung, S.L., 2009b. Geochronology and petrogenesis of granitic rocks in Gangdese batholith, southern Tibet. Sci. China Earth Sci. 52, 1240–1261.
Jiang, S.Y., Zhao, K.D., Jiang, Y.H., Ling, H.F., Ni, P., 2006. New type of tin mineralization related to granite in South China: evidence from mineral chemistry, element and isotope geochemistry. Acta Petrol. Sin. 22, 2509–2516 (in Chinese with English abstract).
Jiang, S.Y., Zhao, K.D., Jiang, Y.H., Dai, B.Z., 2008. Characteristics and genesis of Mesozoic A-type granites and associated mineral deposits in the Southern Hunan and Northern Guangxi provinces along the Shi-Hang belt, South China. Geol. J. China Univers. 14, 496–509 (in Chinese with English abstract).
Jiang, B., Gong, Q.J., Zhang, J., Ma, N., 2012. Late Cretaceous aluminium A-type granites and its geological significance of Dasongpo Sn deposit, Tengchong. West Yunnan. Acta Petrol. Sin. 28, 1477–1492 (in Chinese with English abstract).
Jiang, H., Li, W.Q., Jiang, S. Yong, Wang, H., Wei, X., Peng, 2017. Geochronological, geochemical and Sr-Nd-Hf isotopic constraints on the petrogenesis of Late Cretaceous A-type granites from the Sibumasu Block, Southern Myanmar, SE Asia. Lithos 268–271, 32–47.
Kapp, P., Yin, A., Harrison, T.M., Ding, L., 2005. Cretaceous-Tertiary shortening, basin development, and volcanism in central Tibet. Geol. Soc. Am. Bull. 117, 865–878.
King, P.L., Chappell, B.W., Allen, C.M., White, A.J.R., 2001. Are A-type granites the high-temperature felsic granites? Evidence from fractionated granites of the Wangrah Suite. Aust. J. Earth Sci. 48, 501–514.
Konopelko, D., Seltmann, R., Biske, G., Lepekhina, E., Sergeev, S., 2009. Possible source dichotomy of contemporaneous post-collisional barren I-type versus tin-bearing A-type granites, lying on opposite sides of the South Tien Shan suture. Ore Geol. Rev. 35, 206–216.
Lamarao, C.N., Pinho, S.C.C., Paiva, A.L., Galarza, M.A., 2012. Mineralogy and geochemistry of the Paleoproterozoic, tin-mineralized Bom Jardim granite of the Velho Guilherme Suite, eastern Amazonian craton. J. South Am. Earth Sci. 38, 159–173.
Leech, M.L., Singh, S., Jain, A.K., Klemperer, S.L., Manickavasagam, R.M., 2005. The onset of India-Asia continental collision: early, steep subduction required by the timing of UHP metamorphism in the western Himalaya. Earth Planet. Sci. Lett. 234, 83–97.
Li, Z.L., Hu, R.Z., Yang, J.S., Peng, J.T., Li, X.M., Bi, X.W., 2007. He, Pb and S isotopic constraints on the relationship between the A-type Qitianling granite and the Furong tin deposit, Hunan Province, China. Lithos 97, 161–173.
Li, G., Hua, R., Zhang, W., Hu, D., Wei, X., Huang, X.E., Xie, L., Yao, J., Wang, X., 2011. He-Ar isotope composition of pyrite and Wolframite in the Tieshanlong Tungsten Deposit, Jiangxi, China: implications for fluid evolution. Res. Geol. 61, 356–366.
Li, Z.H., Lin, S.L., Cong, F., Zou, G.F., Xie, T., 2012. U-Pb dating and Hf isotopic compositions of quartz diorite and monzonitic granite from the Tengchong-Lianghe Block, Western Yunnan, and its geological implications. Acta Geosci. Sin. 86, 1047–1062 (in Chinese with English abstract).
Lin, I.J., Chung, S.L., Chu, C.H., Lee, H.Y., Gallet, S., Wu, G.Y., Ji, J.Q., Zhang, Y.Q., 2012. Geochemical and Sr-Nd isotopic characteristics of Cretaceous to Paleocene granitoids and volcanic rocks, SE Tibet: petrogenesis and tectonic implications. J. Asian Earth Sci. 53, 131–150.
Lin, J.Z., Cao, H.W., Zhang, T.T., Liu, R.P., Xiao, C.X., Yang, K., 2015. Geochemical characteristics and zircon U-Pb dating for A-type granites in Lailishan, Tengchong, Southeastern Tibet and its Tectonic Significance. Geotect. Metall. 5, 959–971.
Liu, G.L., Qin, D.X., Fan, Z.G., 2005. Tin resource and its sustainable developing in Yunnan Province. Conserv. Util. Miner. Res. 9–13 (in Chinese with English abstract).
Loiselle, M.C., Wones, D.R., 1979. Characteristics and origin of anorogenic granites. Geol. Soc. Am. Bull. Abstr. Prog. 11 (468).
Luo, J.L., Yang, Y.H., Zhao, Z., Chen, J.C., Yang, J.Z., 1994. Evolution of the Tethys in Western Yunnan and Mineralization for Main Metal Deposits. Geological Publishing House, Beijing, pp. 1–271 (in Chinese with English abstract).
Mao, J.W., Zhang, S.L., Rossi, P., 1987. The tin-granites and their relation to mineralization in Tengchong, Yunnan. Acta Petrol. Sin. 32–43 (in Chinese with English abstract).
Mao, J.W., Li, X.F., Chen, W., Lan, X.M., Wei, S.L., 2004. ^{40}Ar-^{39}Ar dating of tin ores and related granite in Furong tin orefield Hunan Province, and its geodynamic significance. Miner. Deposits 23, 164–175 (in Chinese with English abstract).
Metcalfe, I., 1984. Stratigraphy, palaeontology and palaeogeography of the Carboniferous of Southeast Asia. Mem. Geol. Soc. Fr. 147, 107–118.
Metcalfe, I., 1988. Origin and assembly of Southeast Asian continental terranes. In: Audley-Charles, M.G., Hallam, A. (Eds.), Gondwana and Tethys. Special Publications, 37. Geological Society, London, pp. 101–118.
Metcalfe, I., 1996. Gondwanaland dispersion, Asian accretion and evolution of eastern Tethys. Aus. J. Earth Sci. 43, 605–623.
Metcalfe, I., 2000. The Bentong-Raub Suture Zone. J. Asian Earth Sci. 18, 691–712.
Metcalfe, I., 2002. Permian tectonic framework and palaeogeography of SE Asia. J. Asian Earth Sci. 20, 551–566.
Metcalfe, I., 2013. Gondwana dispersion and Asian accretion: tectonic and palaeogeographic evolution of eastern Tethys. J. Asian Earth Sci. 66, 1–33.
Mo, X.X., Hou, Z.Q., Niu, Y.L., Dong, G.C., Qu, X.M., Zhao, Z.D., Yang, Z.M., 2007. Mantle contributions to crustal thickening during continental collision: evidence from Cenozoic igneous rocks in southern Tibet. Lithos 96, 225–242.
Mo, X.X., Niu, Y.L., Dong, G.C., Zhao, Z.D., Hou, Z.Q., Zhou, S., Ke, S., 2008. Contribution of syncollisional felsic magmatism to continental crust growth: A case study of the Paleogene Linzizong volcanic Succession in southern Tibet. Chem. Geol. 250, 49–67.
Moura, M.A., Botelho, N.F., de Mendonca, F.C., 2007. The indium-rich sulfides and rare arsenates of the Sn-In-mineralized mangabeira A-type granite, central Brazil. Can. Mineral. 45, 485–496.

Neto, A.C.B., Pereira, V.P., Ronchi, L.H., de Lima, E.F., Frantz, J.C., 2009. The world-class Sn, Nb, Ta, F (Y, REE, Li) deposit and the massive cryolite associated with the albite-enriched facies of the Madeira A-type granite, Pitinga mining district, Amazonas State, Brazil. Can. Mineral. 47, 1329–1357.
Ng, S.W.P., Whitehouse, M.J., Searle, M.P., Robb, L.J., Ghani, A.A., Chung, S., Oliver, G.J.H., Sone, M., Gardiner, N.J., Roselee, M.H., 2015. Petrogenesis of Malaysian granitoids in the Southeast Asian tin belt: Part 1. Geochemical and Sr-Nd isotopic characteristics. Geol. Soc. Am. Bull. 127, 1209–1237.
Norman, D.I., Musgrave, J.A., 1994. N_2-He-Ar composition in fluid inclusion: indicators of fluid source. Geochimi. Cosmochim. Acta 58, 1119–1132.
Ohmoto, H., 1972. Systematics of sulfur and carbon isotopes in hydrothermal ore deposits. Econ. Geol. 67, 551–578.
Ohmoto, H., Rye, R.O., 1979. Isotope of sulfur and carbon. In: Barnes, H.L. (Ed.), Geochemistry of Hydrothermal Ore Deposits, second ed. John Wileyand Sons, New York, pp. 509–567.
Oxburgh, E.R., O'Nions, R.K., Hill, R.I., 1986. Helium isotopes in sedimentary basins. Nature 324, 632–635.
Ozima, M., Podosek, F.A., 2001. Noble gas geochemistry. Cambridge University Press (367 pp.).
Patiño Douce, A.E., 1997. Generation of metaluminous A-type granites by low-pressure melting of calc-alkaline granitoids. Geology 25, 743–746.
Payolla, B.L., Bettencourt, J.S., Kozuchi, M., Leite, W.B., Fetter, A.H., Van Schmus, W.R., 2002. Geological evolution of the basement rocks in the east-central part of the Rondonia Tin Province, SW Amazonian craton, Brazil: U-Pb and Sm-Nd isotopic constraints. Precambrian Res. 119, 141–169.
Peng, J.T., Hu, R.Z., Bi, X.W., Dai, T.M., Li, Z.L., Li, X.M., Shuang, Y., Yuan, S.D., Liu, S.R., 2007. $^{40}Ar/^{39}Ar$ isotopic dating of tin mineralization in Furong deposit of Hunan Province and its geological significance. Miner. Deposits 26, 237–248 (in Chinese with English abstract).
Qu, X.M., Hou, Z.Q., Zhou, S.G., 2002. Geochemical and Nd, Sr isotopic study of the post-orogenic granites in the Yidun arc belt of northern Sanjiang region, southwestern China. Res. Geol. 52, 163–172.
Qu, X.M., Wang, R.J., Xin, H.B., Jiang, J.H., Chen, H., 2012. Age and petrogenesis of A-type granites in the middle segment of the Bangonghu-Nujiang suture, Tibetan plateau. Lithos 146, 264–275.
Schwartz, M.O., Rajah, S.S., Askury, A.K., Putthapiban, P., 1995. The Southeast-Asian tin belt. Earth-Sci. Rev. 38, 95–286.
Searle, M.P., Windley, B.F., Coward, M.P., Cooper, D.J.W., Rex, A.J., Rex, D., Li, T.D., Xiao, X.C., Jan, M.Q., Thakur, V.C., Kumar, S., 1987. The closing of Tethys and the tectonics of the Himalaya. Geol. Soc. Am. Bull. 98, 678–701.
Searle, M., Corfield, R.I., Stephenson, B., McCarron, J., 1997. Structure of the North Indian continental margin in the Ladakh-Zanskar Himalayas: implications for the timing of obduction of the Spontang ophiolite, India-Asia collision and deformation events in the Himalaya. Geol. Mag. 134, 297–316.
Şengör, A.M.C., 1979. Mid-Mesozoic closure of Permo-Triassic Tethys and its implications. Nature 279, 590–593.
Şengör, A.M.C., 1984. The Cimmeride orogenic system and the tectonics of Eurasia. Geological Society of America, Special Paper, 195. Geol. Soc. Am. Bull. 195.
Şengör, A.M.C., 1987. Tectonics of the tethysides: orogenic collage development in a collisional setting. Ann. Rev. Earth Planet. Sci. 15, 213–244.
Shi, L, Chen, J.C., Wu, S.L., Peng, X.J., Tang, S.C., 1989. Metallogenic Regularity of Western Yunnan Sn Belt. Geological Publishing House, Beijing 200 pp (in Chinese).
Shi, L., Tang, L.D., Zhao, M., Zhang, W.P., 1991. Types of primary tin ore deposit and metallogenic mechanism in Tengchong-Lianghe area. Yunnan Geol. 10, 191–322.
Simmons, S.F., Sawkins, F.J., Schlutter, D.J., 1987. Mantle-derived helium in two Peruvian hydrothermal ore deposits. Nature 329, 429–432.
Smith, P.E., Evensen, N.M., York, D., Szatmari, P., Oliveira, D.C., 2001. Single-crystal ^{40}Ar-^{39}Ar dating of pyrite: no fool's clock. Geology 29, 403–406.
Stemprok, M., 1990. Solubility of tin, tungsten and molybdenum oxides in felsic magmas. Minera. Deposita 25, 205–212.
Stuart, F.M., Turner, G., 1992. The abundance and isotopic composition of the noble gases in ancient fluids. Chem. Geol. 101, 97–109.
Stuart, F.M., Turner, G., Duckworth, R.C., Fallick, A.E., 1994. Helium isotopes as tracers of trapped hydrothermal fluids in ocean-floor sulfides. Geology 22, 823–826.
Stuart, F.M., Burnard, P.G., Taylor, R.P., Turner, G., 1995. Resolving mantle and crustal contributions to ancient hydrothermal fluids: He/Ar isotopes in fluid inclusions from Dae Hwa W\Mo mineralisation, South Korea. Geochim. Cosmochim. Acta 59, 4663–4673.
Sun, X.M., Zhang, Y., Xiong, D.X., Sun, W.D., Shi, G.Y., Zhai, W., Wang, S.W., 2009. Crust and mantle contributions to gold-forming process at the Daping deposit, Ailaoshan gold belt, Yunnan, China. Ore Geol. Rev. 36, 235–249.
Tang, L.D., 1992. Discussion to genitic type of Lailishan tin deposit in Tengchong-Lianghe region. Yunnan Geol. 11, 283–288 (in Chinese with English abstract).
Taylor, H.P., 1974. The application of oxygen and hydrogen isotope studies to problems of hydrothermal alteration and ore deposition. Econ. Geol. 69, 843–883.
Taylor, R.G., 1976. Porhyry tin deposits in Bolivia. Econ. Geol. 71, 1064–1065.
Taylor, R.G., 1979. Geology of Tin Deposits. Elsevier Scientific Publishing Company, Amsterdam, pp. 1–543.
Taylor, J.R., Wall, V.J., 1992. The behavior of tin granitoid magmas. Econ. Geol. Bulle. Soc. Econ. Geol. 87, 403–420.
Taylor, J.R., Wall, V.J., 1993. Cassiterite solubility, tin speciation, and transport in a magmatic aqueous phase. Econ. Geol. Bull. Soc. Econ. Geol. 88, 437–460.
Turner, G., Burnard, P.B., Ford, J.L., Gilmour, J.D., Lyon, I.C., Stuart, F.M., 1993a. Tracing fluid sources and interaction: discussion. Phys. Sci. Eng. 344, 127–140.
Turner, S., Hawkesworth, C., Liu, J.Q., Rogers, N., Kelley, S., Vancalsteren, P., 1993b. Timing of Tibetan uplift constrained by analysis of volcanic rocks. Nature 364, 50–54.
Ueno, K., 2003. The Permian fusulinoidean faunas of the Sibumasu and Baoshan blocks: their implications for the palaeogeographic and palaeoclimatologic reconstruction of the Cimmerian Continent. Palaeoecology 193, 1–24.
Wang, Y.J., Xing, X.W., Cawood, P.A., Lai, S.C., Xia, X.P., Fan, W.M., Liu, H.C., Zhang, F.F., 2013. Petrogenesis of early Paleozoic peraluminous granite in the Sibumasu Block of SW Yunnan and diachronous accretionary orogenesis along the northern margin of Gondwana. Lithos 182–183, 67–85.
Wen, D.R., Liu, D.Y., Chung, S.L., Chu, M.F., Ji, J.Q., Zhang, Q., Song, B., Lee, T.Y., Yeh, M.W., Lo, C.H., 2008. Zircon SHRIMP U-Pb ages of the Gangdese Batholith and implications for Neotethyan subduction in southern Tibet. Chem. Geol. 252, 191–201.
Whalen, J.B., Currie, K.L., Chappell, B.W., 1987. A-type granites: geochemical characteristics, discrimination and petrogenesis. Contrib. Mineral. Petrol. 95, 407–419.
Wu, F.Y., Sun, D.Y., Li, H.M., Jahn, B.M., Wilde, S., 2002. A-type granites in northeastern China: age and geochemical constraints on their petrogenesis. Chem. Geol. 187, 143–173.
Wu, F.Y., Li, X.H., Yang, J.H., Zheng, Y.F., 2007. Discussions on the petrogenesis of granites. Acta Petrol. Sin. 23, 1217–1238 (in Chinese with English abstract).
Wu, F.Y., Huang, B.C., Ye, K., Fang, A.M., 2008. Collapsed Himalayan-Tibetan orogen and the rising Tibetan Plateau. Acta Petrol. Sin. 24, 1–30 (in Chinese with English abstract).
Wu, L.Y., Hu, R.Z., Peng, J.T., Bi, X.W., Jiang, G.H., Chen, H.W., Wang, Q.Y., Liu, Y.Y., 2011. He and Ar isotopic compositions and genetic implications for the giant Shizhuyuan W-Sn-Bi-Mo deposit, Hunan Province, South China. Int. Geol. Rev. 53, 677–690.
Xu, H., Zhang, M.H., Zhu, S.Z., 2010. An approach to geological features and genesis for the Lianghe Sn deposit. Acta Geol. Sin. 30, 206–209 (in Chinese with English abstract).
Xu, Y.G., Yang, Q.J., Lan, J.B., Luo, Z.Y., Huang, X.L., Shi, Y.R., Xie, L.W., 2012. Temporal-spatial distribution and tectonic implications of the batholiths in the Gaoligong-Tengliang-Yingjiang area, western Yunnan: constraints from zircon U-Pb ages and Hf isotopes. J. Asian Earth Sci. 53, 151–175.
Xu, L.L., Bi, X.W., Hu, R.Z., Tang, Y.Y., Jiang, G.H., Qi, Y.Q., 2014. Origin of the ore-forming fluids of the Tongchang porphyry Cu-Mo deposit in the Jinshajiang-Red River alkaline igneous belt, SW China: constraints from He, Ar and S isotopes. J. Asian Earth Sci. 79, 884–894.
Yang, Q.J., Xu, Y.G., Huang, X.L., Luo, Z.Y., Shi, Y.R., 2009. Geochronology and geochemistry of granites in the Tengliang area, western Yunnan: tectonic implication. Acta Petrol. Sin. 25, 1092–1104 (in Chinese with English abstract).
Yang, G., Li, Y., Si, G., Wu, H., Jin, Z., 2010. LA-ICP-MS Zircon U-Pb Age, Geochemistry and genesis of the aluminous A-type granite in Beilekuduke, Xinjiang. Acta Geol. Sin. 84, 1759–1769 (in Chinese with English abstract).
Yin, A., Harrison, T.M., 2000. Geologic evolution of the Himalayan-Tibetan orogen. Annu. Rev. Earth Planet. Sci. 28, 211–280.
York, D., Masliwec, A., Kuybida, P., Hanes, J.E., Hall, C.M., Kenyon, W.J., Spooner, E.T.C., Scott, S.D., 1982. $^{40}Ar/^{39}Ar$ dating of pyrite. Nature 300, 52–53.
Yue, Y.H., Ding, L., 2009. $^{40}Ar/^{39}$ Ar geochronology, geochemical characteristics and genesis of the Linzhou basic dikes, Tibet. Acta Petrol. Sin. 22, 855–866.
Zaw, K., 1990. Geological, petrogical and geochemical characteristics of granitoid rocks in Burma: with special reference to the associated W-Sn mineralization and their tectonic setting. J. Southeast Asian Earth Sci. 4, 293–335.
Zhai, D., Liu, J.J., Ripley, E.M., Wang, J.P., 2015. Geochronological and He-Ar-S isotopic constraints on the origin of the Sandaowanzi gold-telluride deposit, northeastern China. Lithos 213, 338–352.
Zhang, S.L., 1986. Geological setting and ore types of the Tengchong tin ore belt in Yunnan province. Mineral Deposits 5, 19–26 (in Chinese with English abstract).
Zhang, Y., Jin, C.H., Fan, W.Y., Zhang, H., Shen, Z.W., Gao, J.H., Cheng, W.B., 2013. Geochemical characteristics and classification of granites related to tin deposits in the Tengchong area, Southwest China. Acta Geol. Sin. 12, 1853–1863 (in Chinese with English abstract).
Zhang, H., Sheng, J.F., Dong, G.C., Liu, S.Q., Wang, D.L., 2017. Mineralogical research and H-O isotopic characteristics of the Lailishan tin deposit in Yunnan Province. Acta Petrol. Mineral. 1, 48–59 (in Chinese with English abstract).
Zhao, X.F., Zhou, M.F., Li, J.W., Wu, F.Y., 2008. Association of Neoproterozoic A- and I-type granites in South China: implications for generation of A-type granites in a subduction-related environment. Chem. Geol. 257, 1–15.
Zhao, K.D., Jiang, S.Y., Chen, W.F., Chen, P.R., Ling, H.F., 2013. Zircon U-Pb chronology and elemental and Sr-Nd-Hf isotope geochemistry of two Triassic A-type granites in South China: implication for petrogenesis and Indosinian transtensional tectonism. Lithos 160, 292–306.
Zhu, B., Kidd, W.S.F., Rowley, D.B., Currie, B.S., Shafique, N., 2005. Age of initiation of the India-Asia collision in the east-central Himalaya. J. Geol. 113, 265–285.
Zhu, D.C., Zhao, Z.D., Niu, Y.L., Mo, X.X., Chung, S.L., Hou, Z.Q., Wang, L.Q., Wu, F.Y., 2011. The Lhasa Terrane: record of a microcontinent and its histories of drift and growth. Earth Planet. Sci. Lett. 301, 241–255.
Zhu, M.T., Zhang, L.C., Wu, G., Jin, X.D., Xiang, P., Li, W.J., 2013a. Zircon U-Pb and pyrite Re-Os age constraints on pyrite mineralization in the Yinjiagou deposit, China. Int. Geol. Rev. 55, 1616–1625.
Zhu, D.C., Zhao, Z.D., Niu, Y.L., Dilek, Y., Hou, Z.Q., Mo, X.X., 2013b. The origin and pre-Cenozoic evolution of the Tibetan Plateau. Gondwana Res. 23, 1429–1454.